Computers and Geotechnics 128 (2020) 103618

Contents lists available at ScienceDirect

Computers and Geotechnics

journal homepage: www.elsevier.com/locate/compgeo

Research Paper

Extension of Winkler's solution to non-isothermal conditions for capturing the behaviour of plane geostructures subjected to thermal and mechanical actions

Jacopo Zannin[a,*], Alessandro F. Rotta Loria[b], Qazim Llabjani[a], Lyesse Laloui[a]

[a] Swiss Federal Institute of Technology in Lausanne, EPFL, Laboratory of Soil Mechanics, Station 18, 1015 Lausanne, Switzerland
[b] Northwestern University, Department of Civil and Environmental Engineering, Mechanics and Energy Laboratory, 2145 Sheridan Road, Evanston, IL 60208-3109, USA

ARTICLE INFO

Keywords:
Soil-structure interaction
Analytical modelling
Winkler solution
Thermomechanical behaviour

ABSTRACT

Before this study, no analytical models had been made available for describing the behaviour of plane geostructures subjected to thermal and mechanical actions. This knowledge gap notably represented a limitation for investigations about the behaviour of so-called energy geostructures, which are subjected to the considered actions due to their geothermal heat exchanger and structural support roles. In this study, the first analytical model that allows describing the behaviour of plane geostructures subjected to thermal and mechanical actions is presented. This model extends Winkler's solution to non-isothermal conditions for quantifying the effects of temperature variations, axial loads, transversal loads and bending moments applied to plane geostructures resting on an elastic soil mass. The model is applied to the analysis of an elementary unit represented by a single beam as well as to more complex plane geostructures using the superposition principle. The obtained results are compared with predictions deriving from more rigorous yet time-consuming numerical analyses, showing close agreement. This result makes the developed analytical model a useful tool for scientific and engineering purposes, paving the way for future developments in this scope.

1. Introduction

The behaviour of geostructures critically depends on their interaction with the ground. Conventionally, interactions between geostructures and the ground have mainly been associated with mechanical actions. Currently, a rising number of situations involve geostructures that are subjected to a variety of multiphysical actions. When dealing with so-called energy geostructures, which involve dual structural support and geothermal heat exchanger role, thermal and mechanical actions (that must be considered for analysis and design purposes) are typically encountered (Laloui and Rotta Loria, 2019).

A variety of modelling approaches can be employed to address the interaction occurring between geostructures and the ground. Examples of these approaches include analytical and numerical models, with the former being preferred to the latter especially at early stages of analysis and design (e.g., geotechnical and structural) due to their simplified yet representative description of reality.

Since the 18th century, Coulomb (1776) and Winkler (1867) have addressed the analytical modelling of the interaction between geostructures and the surrounding ground. Winkler's *theory of subgrade reaction* has been developed resorting to the previous investigations and employed for analysing problems related to horizontal footings (Terzaghi, 1955), retaining walls (Ménard and Bourdon, 1965) and piles (Coyle and Reese, 1966; Galin,1943). The analytical solution associated with Winkler's theory describes a beam foundation resting on a soil mass composed by a series of closely spaced, linear elastic and independent springs, whose stiffness (called modulus of subgrade reaction) governs the relationship between the pressure exerted by the soil to the foundation and the deflection. Winkler's solution can be applied to describe the behaviour of plates and beams, although limitations in the resulting predictions are typically observed due to the lack of continuity at the foundation edges. A variety of models have been proposed to improve Winkler's solution with respect to the limitations above. In these models, in addition to the parameter associated with the stiffness of the spring, the soil is described using one or two parameters that include the effects of additional flexural elements, virtual shear layers, pre-tensioned membranes, etc. (Hétenyi, 1946, 1950; Kerr, 1965; Reissner, 1937). A description of such models has been proposed by Hétenyi (1946) and Selvadurai (1979). Models based on Winkler's solution can thus include one, two, or three parameters. In

* Corresponding author.
E-mail address: jacopo.zannin@epfl.ch (J. Zannin).

https://doi.org/10.1016/j.compgeo.2020.103618
Received 16 January 2020; Received in revised form 15 April 2020; Accepted 20 April 2020

general, the subgrade reaction modulus included in Winkler's solution can be related in a straightforward manner to the elastic properties of soils. In contrast, the second and third parameters included in the models above are sometimes difficult to estimate because they do not necessarily have a physical meaning. For this reason, the basic formulation of Winkler's solution is often employed for practical purposes to provide approximate yet representative information.

Applications of analytical models based on Winkler's solution typically address horizontal footings and vertical retaining structures. Substantial differences among the previous two applications reside in the determination and calibration of the Winkler's subgrade reaction modulus. For horizontal footings, several theoretical, semi-empirical and empirical definitions are available in the literature (e.g., Terzaghi, 1955; Selvadurai, 1979; Barden, 1962, 1963; Biot, 1937; Galin, 1943; Vesic, 1961a, 1961b, Vesic and Johnson, 1963; Meyerhof and Baikie, 1963). For vertical retaining structures, the complexities of the problem geometry make theoretical estimations complicated and extensive validations of semi-empirical and empirical procedures against field testing are often necessary (e.g., Terzaghi, 1955; Ménard and Bourdon, 1965; Balay, 1984; Fages and Bouyat, 1971; Monnet, 1994; Schmitt, 1995).

Before this study, all of the available analytical models for describing the interaction between plane geostructures and the ground allowed a description of the influence of only mechanical actions. In other words, no analytical soil-structure interaction models for plane geostructures have been made available for capturing the influence of thermal actions, potentially applied in conjunction with mechanical actions. To address this knowledge gap, the present paper proposes the formulation and application of an analytical model based on an extension of Winkler's solution to non-isothermal conditions for describing the behaviour of plane geostructures subjected to thermal and mechanical actions. This model is developed with particular reference to energy geostructures, although it may be employed for the analysis of other relevant problems that are increasingly encountered in science and engineering where earth-contact structures are subjected to thermal and mechanical actions. The analytical model proposed in this study could be employed as an effective alternative to more rigorous yet computationally expensive numerical approaches (Bourne-Webb et al., 2016; Sterpi et al., 2017; Rui and Yin, 2018; Sailer et al., 2019).

In the following, the proposed analytical model is derived and discussed first. Then, the model is applied to the analysis of problems of increasing complexity and the obtained results are compared with those of more rigorous yet time-consuming numerical analyses. Finally, concluding remarks that can be drawn from this work are summarised.

2. Analytical model for plane geostructures subjected to thermal and mechanical actions

2.1. Fundamentals

In this study, a beam is defined as a structural element having one dimension (length, L) that is much greater than the other two (breadth, b, and height, h). Winkler's solution is employed to describe the behaviour of beams resting on an elastic soil mass. Winkler's solution is based on the widely known Euler-Bernoulli theory of beams (circa 1750, as appears in Truesdell (1960). Such a theory allows writing the relationship between the deflection and the loads applied to any beam and obtaining the fourth-order differential equation that governs the problem. In small deformations, Euler-Bernoulli theory involves that straight lines or planes normal to the neutral axis of the beam remain straight and normal to the considered axis after deformation. This feature allows expressing the bending moment proportionally to the second derivative of the deflection.

Based on the previous premises, Winker's solution resorts to the three following hypotheses: (i) The subgrade reaction modulus, k_s, is independent of the pressure and involves the same response for both loading and unloading; (ii) The value of k_s does not vary in space; (iii) The springs work unidirectionally and independently of each other. The previous hypotheses involve the following practical considerations: (i) The soil follows a linear elastic behaviour, which makes the solution representative and suitable for the analysis of limited deformation levels (so-called serviceability conditions); (ii) The soil reaction is uniformly distributed among the springs, which makes the solution unsuitable to describe rigid beams but particularly appropriate to model flexible beams; (iii) Any influence caused by actions in the soil outside the beam length cannot be captured, which makes the solution suitable to provide accurate estimates of action effects along the beam only.

In the following, the adopted sign convention is that of structural mechanics. Positive deflections and rotations are directed downwards and clockwise, respectively, and tensile forces are considered as positive. Unless otherwise specified, reference is made to one-dimensional conditions.

2.2. Influence of thermal and mechanical actions on plane geostructures

Thermal and mechanical actions applied to geostructures result in a variety of effects for the structure and the ground. Thermal actions are typically associated with temperature variations within and around geostructures. Mechanical actions are typically associated with axial loads, transversal loads and bending moments.

The temperature variations caused by thermal actions are generally non-uniform and can be idealised as composed of two contributions (Fig. 1): a constant distribution of temperature variation over the cross-section of the structure, ΔT_a, inducing an axial effect, and a linear distribution of temperature variation over the cross-section of the structure, ΔT_c, inducing a bending effect. These uniform and linear temperature variations can be evaluated as:

$$\Delta T_a = \frac{\Delta T_2 + \Delta T_1}{2} \tag{1}$$

$$\Delta T_c = \frac{\Delta T_2 - \Delta T_1}{2} \tag{2}$$

The axial and bending effects resulting from the previous temperature variations can be associated with a thermally induced axial strain and curvature, respectively. Prevention of these effects results in the development of axial loads and bending moments, respectively. The effects of generally distributed mechanical loads are axial and transversal displacements, rotations of the neutral axis, axial and shear forces, as well as bending moments.

2.3. Degree of freedom: definition for axial and flexural actions

The concept of degree of freedom is a powerful means to address the effects caused by temperature variations applied to geostructures (Rotta Loria and Laloui, 2019): it expresses the development of a relevant physical quantity to its value under free thermal deformation conditions. Before this study, the degree of freedom was applied to describe axial effects caused by thermal actions applied to geostructures (Laloui et al., 2003); in contrast, no applications of this parameter were reported to address flexural effects caused by thermal actions applied to geostructures. In the following, the degree of freedom is defined and employed to address both axial and flexural effects caused by constant and linear distributions of temperature variations applied to geostructures.

A constant distribution of temperature variation, ΔT_a, applied along a geostructure free to move at its ends causes the development of a free thermally induced axial strain, ε_f^{th}, as

$$\varepsilon_f^{th} = \alpha_{th} \Delta T_a \tag{3}$$

where α_{th} is the linear thermal expansion coefficient of the material. A linear distribution of temperature variation applied along a

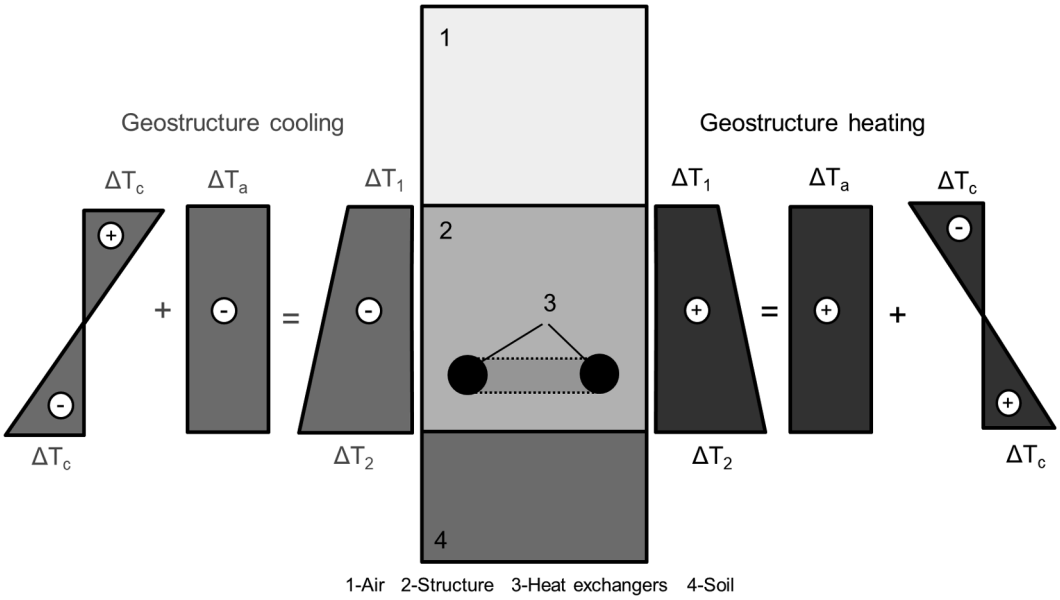

Fig. 1. Idealised schematic of the temperature variation within the cross-section of a plane geostructure interfacing, from one side, the air, and from the other side, the ground. The considered schematic can refer to a slab resting on the ground or to the exposed portion of a retaining wall. ΔT_1 and ΔT_2 refer to the temperature variations at the geostructure-air and geostructure-soil interfaces, respectively.

geostructure free to move at its ends causes the development of a free thermally induced curvature, χ_f^{th}, as

$$\chi_f^{th} = \frac{\alpha_{th}}{I}\int_A y_h \frac{2\Delta T_c}{h} dA = \frac{2\alpha_{th}\Delta T_c}{h} \tag{4}$$

where I is the moment of inertia of the cross-section, A, and y_h is the coordinate along the geostructure height, h.

A partial restraint applied to a geostructure by any given boundary condition (e.g., the presence of the ground and a connected structure) yields to the development of an observed axial deformation and curvature that are a fraction of the ones under free thermal deformation conditions. The previous consideration involves that only a portion of axial deformation and curvature is developed with respect to those under free deformation conditions, while a portion of axial deformation and curvature is blocked.

The previous considerations inherently lead to the definition of degree of freedom. The degree of freedom associated with axial effects, DOF_a, can be defined as:

$$DOF_a = \frac{\varepsilon_o^{th}}{\varepsilon_f^{th}} \quad 0 \le DOF_a \le 1 \tag{5}$$

where ε_o^{th} represents the observed thermally induced axial strain. The degree of freedom associated with flexural effects, DOF_c, can be defined as:

$$DOF_c = \frac{\chi_o^{th}}{\chi_f^{th}} \quad 0 \le DOF_c \le 1 \tag{6}$$

where χ_o^{th} represents the observed thermally induced curvature.

Internal actions develop consequently to the blocked portion of deformations. The restraint of a constant distribution of temperature variation causes a thermally induced axial force. The restraint of linear distribution of temperature variation causes a thermally induced bending moment (which explicates a tensile action at one side of the cross-section and a compressive action at the other side). The observed thermally induced axial force, N_o^{th}, and bending moment, M_o^{th}, caused by the previous temperature variations can be quantified as

$$N_o^{th} = N^{th} = AE\alpha_{th}\Delta T_a(1 - DOF_a) \le N_b^{th} \tag{7}$$

$$M_o^{th} = M^{th} = EI\frac{2\alpha_{th}\Delta T_c}{h}(1 - DOF_c) \le M_b^{th} \tag{8}$$

where N_b^{th} and M_b^{th} are the axial force and bending moment under completely blocked deformation conditions, respectively.

Fig. 2 shows parallelism between the axial and flexural effects caused by constant and linear distributions of temperature variations in a geostructure, highlighting the link between the relevant degree of freedom and the development of deformations and internal actions. The cases of a structure free to deform, completely restrained (i.e., blocked), and partly restrained by varying magnitudes of constraints are considered.

2.4. The analytical model

From Euler-Bernoulli theory, the rotation, $\theta(x)$, the bending moment, $M(x)$ and the shear force, $V(x)$, characterising any infinitely small element of a beam as a consequence of the application of thermal and mechanical actions inducing flexural effects (e.g., non-uniform distribution of temperature variations or distributed loads perpendicular to the beam axis) respectively read

$$\theta(x) \approx \tan\theta(x) = \frac{dy(x)}{dx} \tag{9}$$

$$M(x) = -EI\frac{d^2y(x)}{dx^2} - EI\chi_f^{th} \tag{10}$$

$$V(x) = \frac{dM(x)}{dx} \tag{11}$$

where x is the relevant coordinate axis and y is the deflection. In addition to the previous actions, axial forces, N, can characterise any element of a beam due to the application of thermal and mechanical actions (e.g., uniform distributions of temperature variations or mechanical forces applied normal to the beam transversal cross-section). Consideration of one-dimensional conditions involves neglecting any extension or contraction of the beam within its cross-section due to the considered actions.

Based on the previous considerations, the present model can be formulated by analysing the equilibrium of a beam element resting on an elastic soil of length dx in its deformed configuration (Fig. 3(a)). Vertical equilibrium gives

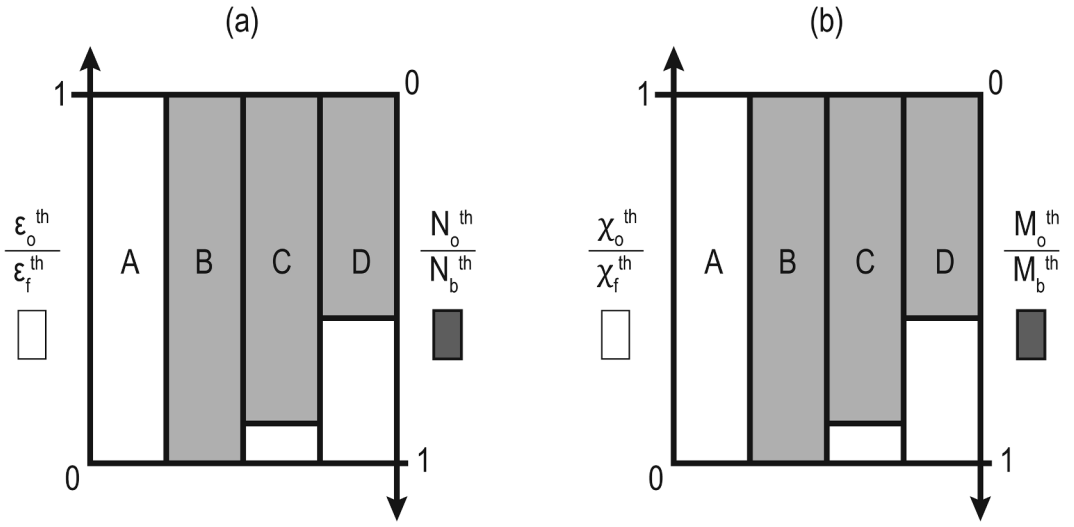

Fig. 2. Qualitative development of deformations and internal actions caused by (a) constant and (b) linear distribution of temperature variations in a geostructure: (A) free case, (B) completely restrained case, (C) partly restrained case with significant prevention of deformations, and (D) less restrained case with less significant prevention of deformations.

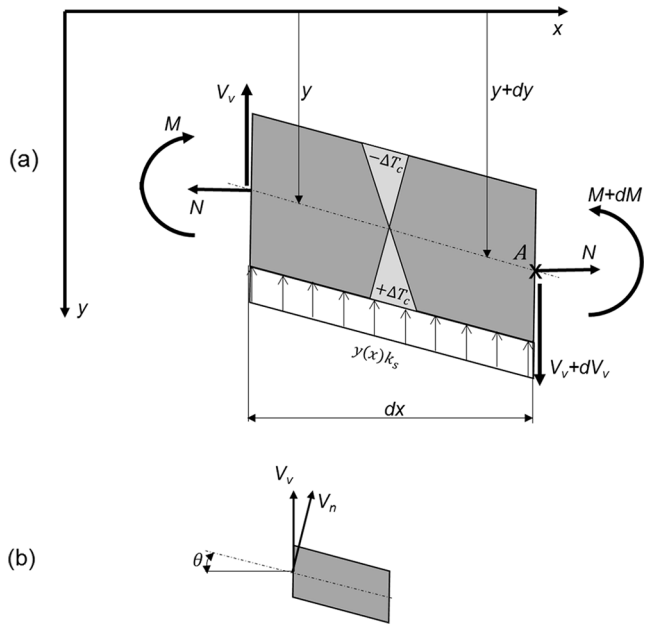

Fig. 3. Schematic of (a) the equilibrium of a beam element of length dx and (b) the geometric decomposition of shear actions.

$$\frac{dV_v}{dx} = y(x)k_s \tag{12}$$

where V_v is the vertical shear force, which can be correlated to the normal shear force, V_n (Fig. 3(b)):

$$V_n = V_v\cos\theta - N\sin\theta \approx V_v - N\frac{dy}{dx} \tag{13}$$

The generalised shear action is evaluated by modifying Eq. (11) to account for the two components of the shear force. The following expression is obtained

$$V(x) = -EI\frac{d^3y(x)}{dx^3} - EI\frac{d\chi_f^{th}}{dx} + N\frac{dy(x)}{dx} \tag{14}$$

The moment equilibrium around point A, divided by dx, can be written as follows (neglecting second-order terms):

$$\frac{dM}{dx} = V_v - N\frac{dy}{dx} \tag{15}$$

Substituting Eqs. (10) into (15), differentiating with respect to x and considering Eq. (12), the differential equation of the elastic line is obtained for this problem:

$$EI\left(\frac{d^4y}{dx^4} + \frac{d\chi^{th2}(x)}{dx^2}\right) - N\frac{d^2y(x)}{dx^2} + k_s y(x) = 0 \tag{16}$$

Eq. (13) has a solution of the type:

$$y(x) = (C_1e^{\alpha x} + C_2e^{-\alpha x})\cos\beta x + (C_3e^{\alpha x} + C_4e^{-\alpha x})\sin\beta x \tag{17}$$

with:

$$\alpha = \sqrt{\lambda^2 + \frac{N}{4EI}} \tag{18}$$

$$\beta = \sqrt{\lambda^2 - \frac{N}{4EI}} \tag{19}$$

where λ is called the characteristic of the system. The term $1/\lambda$ is called the characteristic length, as defined by Hétenyi (1946), and it is a useful parameter to express the problem solution as a function of the non-dimensional parameter , called relative stiffness of the beam. The parameter λ reads

$$\lambda = \sqrt[4]{\frac{k_s}{4EI}} \tag{20}$$

The integration constants, C_1, C_2, C_3 and C_4 can be defined by imposing the boundary conditions and solving the system of Eqs. (9), (10) and (17). The resolution of this system extends the classical Winkler's solution to non-isothermal conditions. In this work, a computer code has been developed to solve this system using the software Wolfram Mathematica 11 (Wolfram Research, 2019).

2.5. Analysis of simple plane geometries

The obtained analytical model can straightforwardly address the effects caused by arbitrary thermal and mechanical actions applied to *simple plane geometries*: geostructures (e.g., beams) of finite dimensions resting on a Winkler-type soil mass that are arbitrarily restrained by boundary conditions and subjected to loading (Fig. 4). This capability resorts to the superposition principle (i.e., an essential constituent of the elastic theory employed herein). Based on this principle, the effects

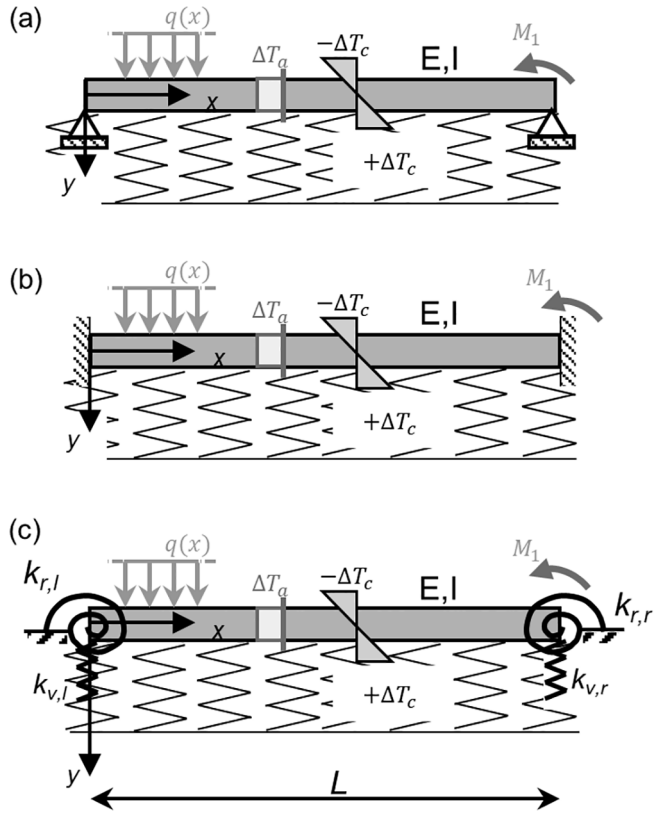

Fig. 4. Examples of simple plane geometries characterised by different boundary conditions: (a) hinged, (b) fixed and (c) partly restrained.

caused by arbitrary combinations of loading actions can be considered as the sum of the effects caused by single actions solved separately. Accordingly, in a situation where one thermal action and one mechanical action are applied, the deflection, rotation, bending moment, shear force and normal force can be considered as made of two contributions: one component caused by the thermal action and another component caused by the mechanical action. The generalised axial force resulting from a thermal and mechanical action can hence be defined for any element of a beam as:

$$N = N^{th} + N^{m} \tag{21}$$

where the superscripts *th* and *m* stand for "thermal" and "mechanical", respectively.

From the previous considerations, it results

$$y(x) = y^{th}(x) + y^{m}(x) \tag{22}$$

$$\theta(x) = \theta^{th}(x) + \theta^{m}(x) \tag{23}$$

$$M(x) = M^{th}(x) + M^{m}(x) \tag{24}$$

$$V(x) = V^{th}(x) + V^{m}(x) \tag{25}$$

The influence of any thermal loading configuration (e.g., a constant or a linear distribution of temperature variation) along the beam can be quantified by imposing the boundary conditions and, consequently, by determining the four integration constants from Eq. (17). The influence of any mechanical loading configuration (e.g., a concentrated mechanical force) can be addressed by employing the method of initial conditions as detailed in Appendix A.

2.6. Analysis of complex plane geometries

The obtained analytical model can also effectively address the effects of arbitrary combinations of thermal and mechanical actions on *complex plane geometries*: geostructures composed by multiple elements mutually connected one another (e.g., cut-and-cover structures, structures involving wall-slab and wall-anchors intersections, mat foundations and multi-floored structures) that are partly or entirely surrounded by a Winkler-type soil mass and subjected to loading (Fig. 5). In the present context, this capability is again related to the superposition principle. Relevant simple plane geometries can be considered as an elementary unit for more complex plane geometries. The effects of thermal and mechanical actions applied to these geometries can be addressed straightforwardly. Once such action effects are obtained, they can be considered as boundary loads for the other unit(s) composing the complex plane geometry. From this perspective, general combinations of thermal and mechanical actions can be solved for all the elementary units constituting any complex geometry, thus yielding a complete procedure for addressing the related response.

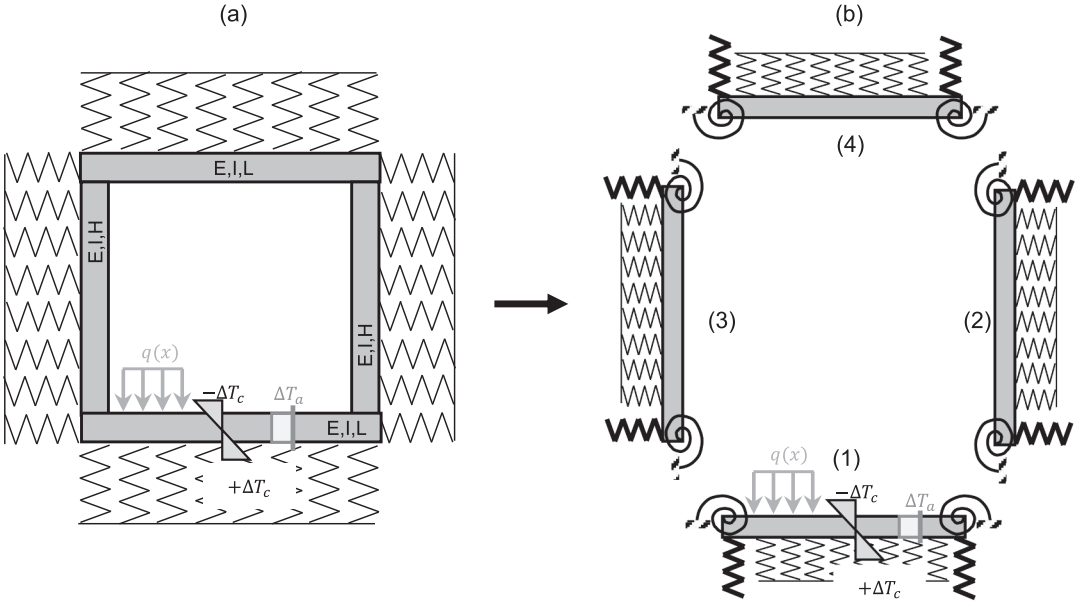

Fig. 5. Example of (a) a complex plane geometry (i.e., a cut-and-cover tunnel) and (b) a related geometrical decomposition approach into four simple plane geometries.

Table 1
Boundary conditions for selected cases.

	Fixed	Hinged	Free	Partly restrained
Conditions	$y(0) = y(L) = 0$	$y(0) = y(L) = 0$	$M(0) = M(L) = 0$	$y(0) = \frac{V(0)}{k_{v,l}}$
	$\theta(0) = \theta(L) = 0$	$M(0) = M(L) = 0$	$V(0) = V(L) = 0$	$\theta(0) = -\frac{M(0)}{k_{r,l}}$
				$y(L) = -\frac{V(L)}{k_{v,r}}$
				$\theta(L) = \frac{M(L)}{k_{r,r}}$

2.7. Boundary conditions

Three possible conditions can characterize the boundaries of beams, such as general geostructures: completely free conditions, completely restrained conditions, or partly restrained conditions (Fig. 4). The most common condition encountered in practice corresponds to a situation wherein beams are partly restrained at their ends (transversal ($k_{v,l}$, $k_{v,r}$) and rotational ($k_{r,l}$, $k_{r,r}$) springs are considered at each end of the structure in such case). In some cases, the restraint characterising beams could be so high that completely restrained conditions may be representative of reality.

A summary of the mathematical formulations allowing to consider the discussed boundary conditions is detailed in Table 1. Consideration of these formulations allows resolving the problems addressed by the obtained analytical model.

2.8. Modulus of subgrade reaction

The modulus of subgrade reaction, k_s, is a crucial parameter to address the response of geostructures. This parameter does not represent an intrinsic characteristic of soils, but it depends on the soil properties, geostructure dimensions, geometry and rigidity, and the spatial distribution of the applied loads (Terzaghi, 1955; Selvadurai, 1979; Delattre, 2001). While Terzaghi (1955) proposed charts for the determination of k_s based on the results of an experimental campaign, other authors proposed empirical relations linking k_s to parameters such as the Young's modulus of soils, E_s, the Poisson's ratio, ν_s, or the foundation breadth, B (Barden, 1962, 1963; Biot, 1937; Galin, 1943; Vesic, 1961a, 1961b; Vesic and Johnson, 1963). Table 2 summarises some widely established empirical formulations to estimate k_s. A practical application of these expressions to determine k_s is presented in Appendix B.

3. Application and validation of the analytical model – simple plane geometries

3.1. General

The literature is rich in investigations addressing with the classical Winkler's solution the effects of mechanical actions (e.g., concentrated and variably distributed forces and moments) on the behaviour of plane geostructures (Hétenyi, 1946; Selvadurai, 1979). In contrast, no investigations addressing the effects of thermal actions have ever been made available before this study. Looking at such a challenge, the proposed extension of Winkler's solution is employed in this section to address the effects of thermal actions (e.g., a unitary linear distribution of temperature variation) on the behaviour of a geostructure characterised by a simple plane geometry. Complementary comments about the effects of thermal (and mechanical) actions on the behaviour of geostructures are eventually reported.

Table 2
Determination of k_s from empirical formulations.

Formula	Reference
$k_s = \frac{0.65E_S}{B(1-\nu_S^2)}$	Barden (1962, 1963)
$k_s = \frac{\pi E_S}{2B(1-\nu_S^2)\ln\frac{L}{B}}$	Galin (1943), recalled in Selvadurai (1979)
$k_s = \frac{1}{B}\left[0.65\sqrt[12]{\frac{E_S B^4}{EI}}\right]\frac{E_S}{1-\nu_S^2}$	Vesic (1961a, 1961b), Vesic and Johnson (1963)
$k_s = \frac{E_S}{B(1-\nu_S^2)}$	Meyerhof and Baikie (1963)
$k_s = \frac{0.95E_S}{B(1-\nu_S^2)}\left[\frac{E_S B^4}{(1-\nu_S^2)EI}\right]^{0.108}$	Biot (1937)

3.2. The problem

In the following, beams characterised by hinged and partly restrained boundary conditions are considered. Perfectly fixed conditions are not treated as they represent a trivial case: displacements are entirely blocked and internal actions are constant everywhere. In other words, the deflection and rotation are equal to zero, and the internal actions reach their constant maximum values by definition of entirely blocked conditions.

Hinged conditions aim at representing the behaviour of beams characterised by connections with an infinite transversal stiffness and zero rotational stiffness at their ends. Such conditions are not usually encountered in practical problems similar to those addressed in this work. Partly restrained conditions aim at representing the behaviour of beams connected with other structural elements that are common in practice (e.g., wall-slab connections, such as for cut-and-cover structures). In the following, when considering partly restrained conditions, symmetric boundary conditions at the ends of the beam are considered: $k_{v,l} = k_{v,r} = k_v$ and $k_{r,l} = k_{r,r} = k_r$. For both of the considered boundary conditions, the subgrade reaction modulus reads $k_s = 10^6 \div 10^8$ N/m^3, aiming at encompassing soft to stiff soils, respectively (Terzaghi, 1955; Selvadurai, 1979). Complementary input parameters characterising the considered problem are presented in Table 3. The rationale of considering a linear distribution of temperature variation of ΔT_c= 1.0 °C is that it provides a unitary response of the modelled problem. In particular, as long as the hypothesis of a reversible response of the soil (and structure) holds, temperature variations of ΔT_c= 10.0 °C and ΔT_c= −1.0 °C, for example, yield to results that are ten times higher and opposite compared to those discussed here, respectively.

To validate the capabilities of the present analytical model in addressing the considered problem, comparisons with the results of numerical models have been made (the details of the numerical models are highlighted in Appendix C). In this context, two problems have been numerically simulated: (i) a beam resting on a spring foundation and (ii) a beam resting on a continuum medium. In the first case, the

Table 3
Input parameters for the modelling of the considered problem.

L [m]	h [m]	B [m]	ΔT_c [°C]	E [Pa]	k_r [Nm/rad]	k_v [N/m]
10.0	0.5	1.0.	1.0	25.0×10^9	1.0×10^9	1.0×10^8

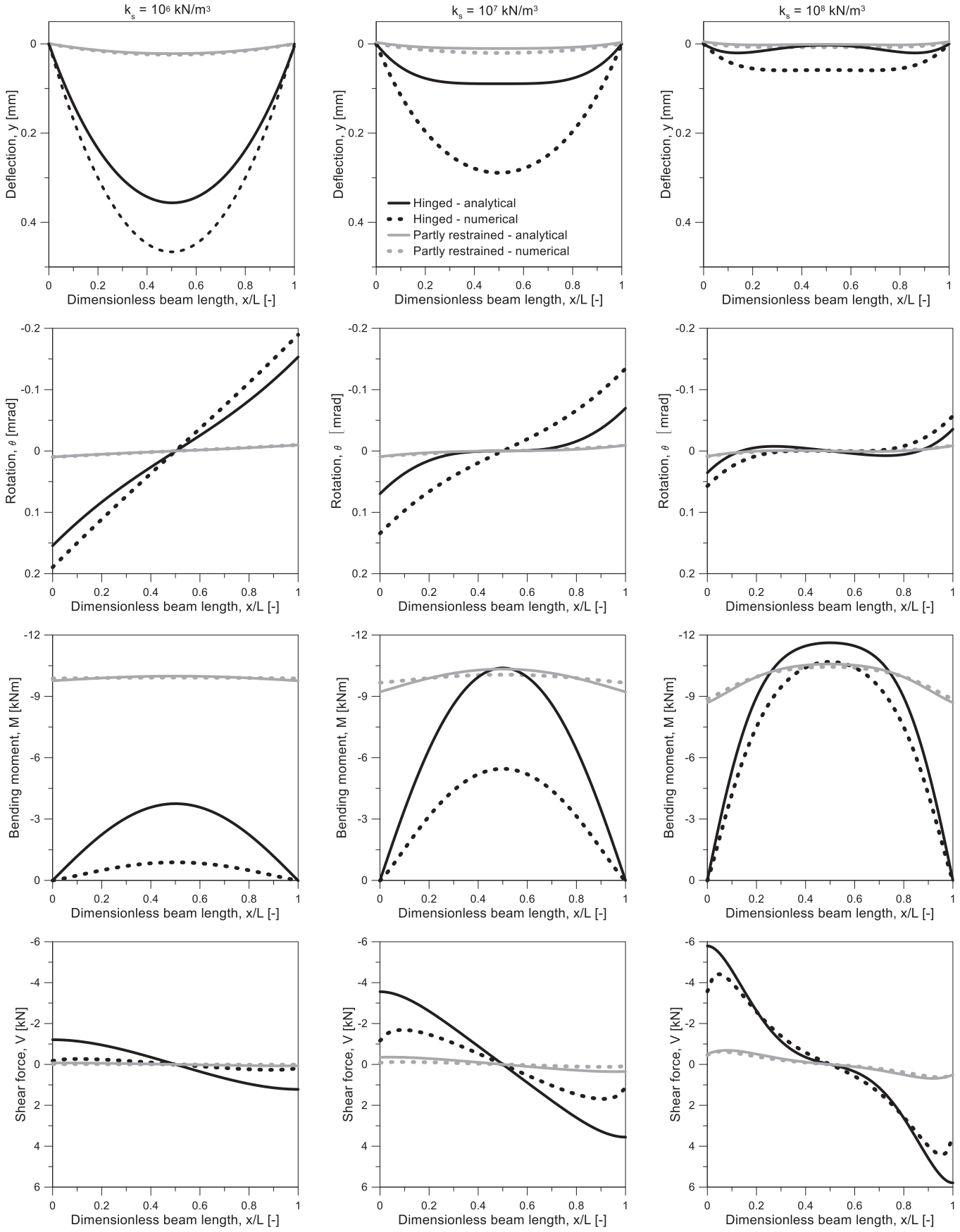

Fig. 6. Thermo-mechanical response of a geostructure resting on different soil conditions and subjected to a linear distribution of temperature variation: comparison between analytical and numerical models.

Table 4
Steps for resolving the cut-and-cover structure employing the proposed analytical model.

Step number	Beam number	Input parameters	Output parameters
1	Base beam (1)	q; ΔT_c	$y_{1,1}(x)$; $\vartheta_{1,1}(x)$; $M_{1,1}(x)$; $V_{1,1}(x)$
2	Right vertical beam (2)	$\vartheta_2(0) = \vartheta_1(L)$ $N_2 = Q_1(L)$	$y_2(x)$; $\vartheta_2(x)$; $M_2(x)$; $V_2(x)$
3	Left vertical beam (3)	$\vartheta_3(0) = \vartheta_1(0)$ $N_3 = Q_1(0)$	$y_3(x)$; $\vartheta_3(x)$; $M_3(x)$; $V_3(x)$
4	Base beam (1)	q; ΔT_c $N_1 = Q_2(0) = -Q_3(L)$	$y_{1,2}(x)$; $\vartheta_{1,2}(x)$; $M_{1,2}(x)$; $V_{1,2}(x)$
5	Top beam (4)	$\vartheta_4(0) = \vartheta_3(H)$ $\vartheta_4(L) = \vartheta_2(H)$ $y_4(0) = y_{1,2}(0)$ $y_4(L) = y_{1,2}(L)$	$y_4(x)$; $\vartheta_4(x)$; $M_4(x)$; $V_4(x)$

analytical and numerical modelling results perfectly match (error of 0%): this result fully validates the capability of the proposed extension of Winkler's solution in capturing the effects of thermal actions with respect to a numerical modelling technique considering the same problem (this capability is also observed for mechanical actions). In the second case, differences between the analytical and numerical modelling results are observed: these differences are discussed in the following.

3.3. Comparison between analytical and numerical modelling results

The comparison between analytical and numerical modelling results is reported in Fig. 6. In the following, considerations related to deflections, rotations and internal actions are reported, and a discussion resorting to the concept of degree of freedom is eventually proposed.

3.3.1. Deflection and rotation

The following considerations apply irrespective of the considered static scheme. For very stiff soils (e.g., $k_s = 10^8$ N/m^3), the relative

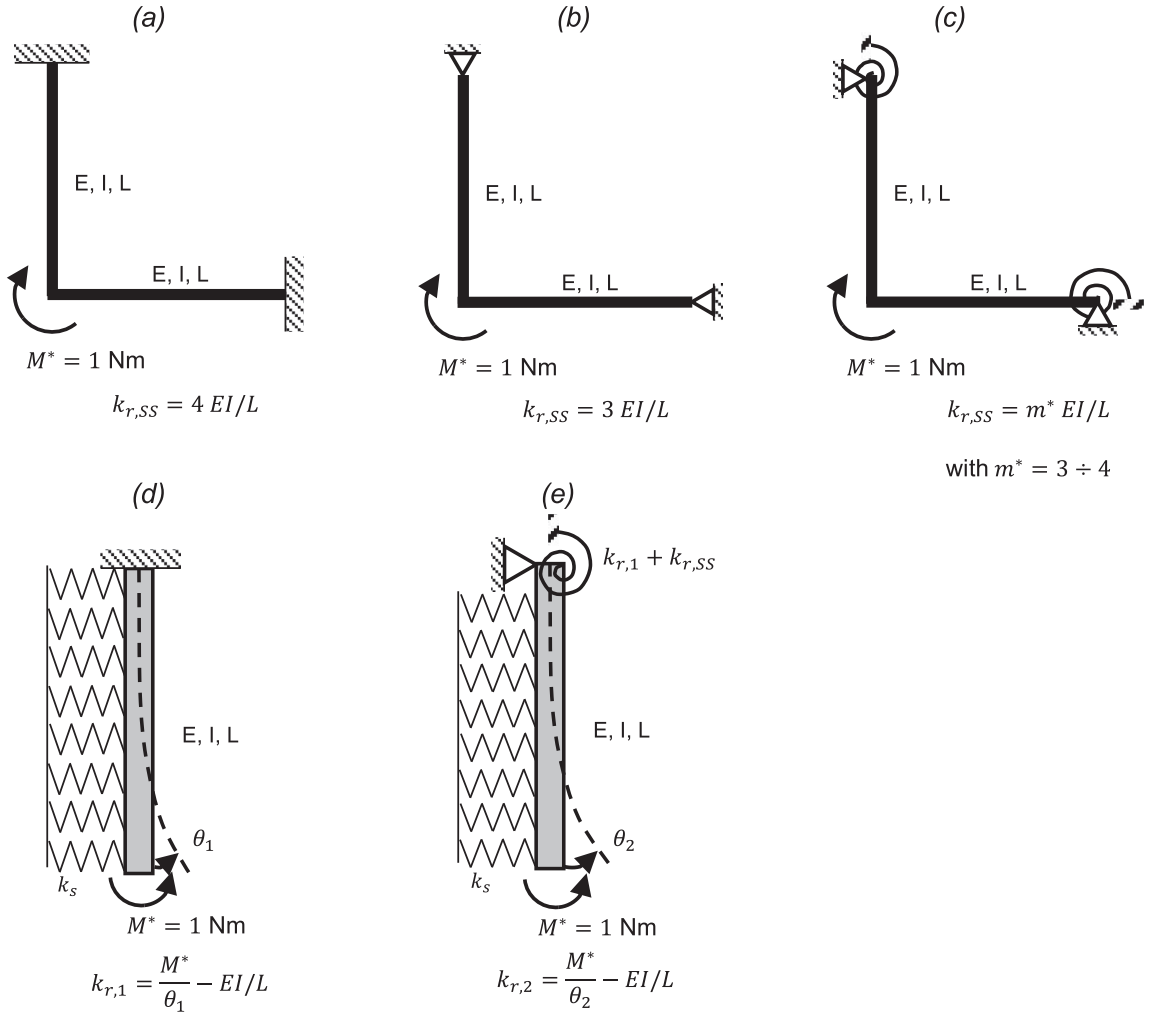

Fig. 7. Determination of the structural rotational stiffness: (a) fixed case, (b) hinged case, (c) partly restrained case. Determination of the soil-structure interaction rotational stiffness: (d) first estimation and (e) final estimation.

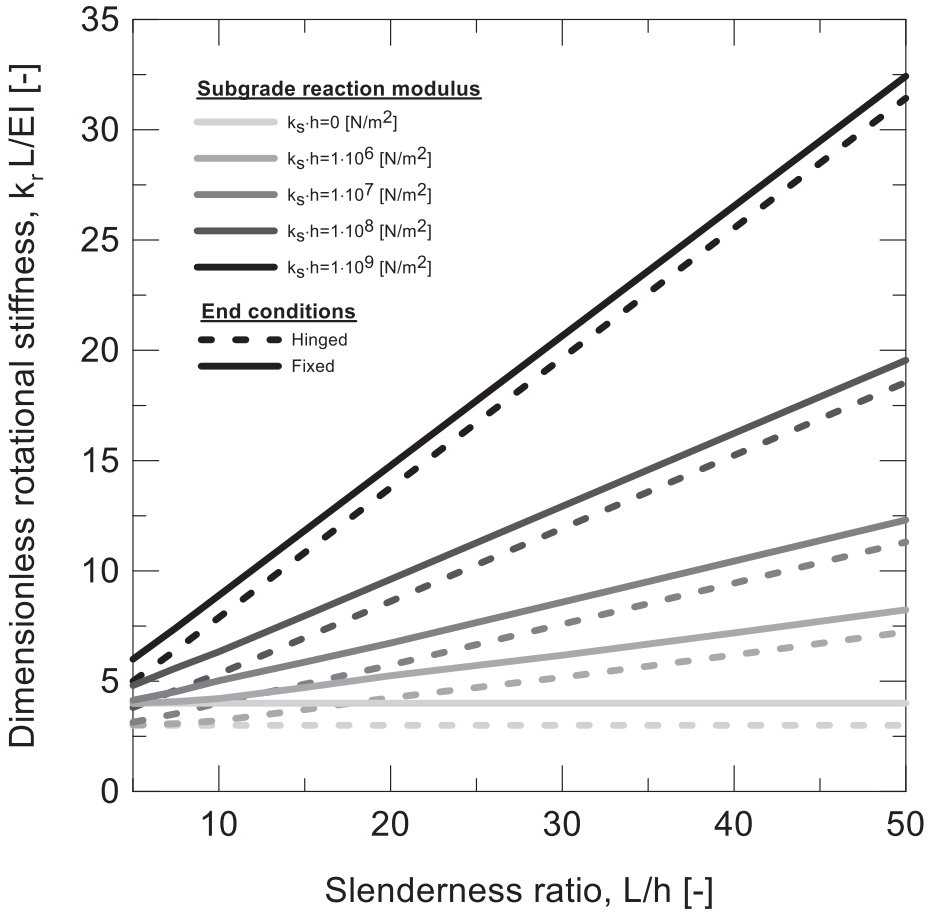

Fig. 8. Relationship between the dimensionless rotational boundary stiffness and the beam geometry.

stiffness λL is significant and thus the deflection is concentrated in the vicinity of the boundaries. It follows that the conditions at one end of the beam do not affect the results at the other end of the beam and the deflection at the mid-span is nearly zero. As suggested by Hétenyi (1946), the solution of this problem can be simplified by a superposition of two semi-infinite beams. For soft soils (e.g., $k_s = 10^6$ N/m^3), the relative stiffness λL is minimal. The maximum deflection takes place at the midpoint of the beam. Following the classification proposed by Hétenyi (1946), the solution of this problem can be found by considering the beam as finite. The maximum values of rotation are recorded at the beam ends. Zero rotation is evaluated at the mid-span of the beam, showing an anti-symmetric distribution.

The following considerations apply with reference to the static scheme. Hinged conditions allow for free rotation at the boundaries and null vertical deflection. Under these conditions, the beam displaces downwards showing a maximum at its mid-span and zero deflection at the boundaries. Rotation is maximum (in absolute value) at the boundaries and becomes equal to zero at the mid-span. At the considered location, the deflection presents a minimum. Partly restrained conditions affect the magnitude of the deflection and rotation. The deformed shape is the same as for hinged conditions, but characterised by a lower magnitude.

By comparing the analytical and numerical modelling results, some remarks can be highlighted. The analytical model suffers from a lack of continuity between the springs and at the sides of the beam. This feature does not characterise the employed numerical model. Therefore, deflection and rotation are generally underestimated by the analytical modelling results compared to the numerical modelling results. Such discrepancies in the results could be partly recovered by employing a two-parameter model such as that reported by Pasternak (1954). The differences between the analytical and numerical modelling results are higher for lower rotational boundary constraints. If there is some rotational stiffness at the boundaries, the results of the analytical model approach the numerical ones.

3.3.2. *Internal actions*

The following considerations apply irrespective of the considered static scheme. Bending moment and shear forces develop because of the applied loads as well as the presence and significance of constraints. In free deformation conditions, a beam subjected to a linear thermal load would deflect downwards and be subjected to zero thermally induced internal actions. In partly or fully restrained conditions, a constraint to the beam bending causes a tensile force in the upper part of the cross-section as a consequence of cooling thermal loading, while a compressive force in the lower part as a consequence of heating thermal loading. The correspondent bending moment shape is towards the beam extrados.

The following considerations apply with reference to the static scheme. By definition of hinged conditions, bending moment is equal to zero at the boundaries of the beam and presents a maximum at the mid-span of the beam. In these conditions, bending is only restrained by the soil reaction. In partly restrained conditions, the observed bending moment follows Eq. (8). The higher the boundary rotational stiffness, the flatter the bending moment distribution. Because of the definition of the shear force (Eq. (11)), shear actions are maximum when high bending moment variations develop along the beam. For flatter bending moment distributions, the shear force approaches zero. It follows that maximum values are recorded at the beam ends for hinged conditions, showing an anti-symmetric distribution.

By comparing the analytical and numerical modelling results, some

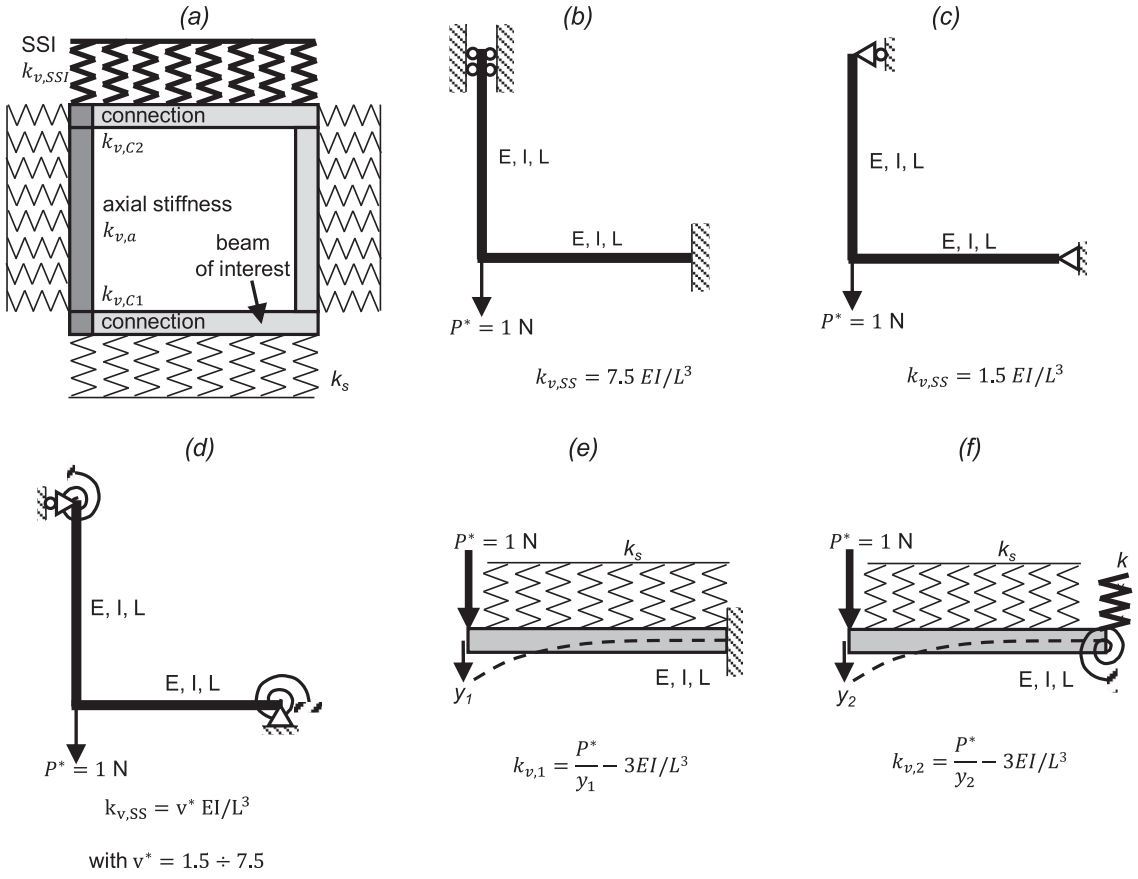

Fig. 9. (a) Components to be considered for the evaluation of the transversal stiffness boundary condition. Determination of the structural transversal stiffness at the connections: (b) fixed case, (c) hinged case, (d) partly restrained case. Determination of the soil-structure interaction transversal stiffness: (e) first estimation and (f) final estimation.

remarks can be highlighted. While the obtained formulation of Winkler's solution underestimates deflections and rotations compared to numerical results considering a continuum soil mass, it overestimates internal actions. The smaller the rotational boundary constraint, the higher the discrepancy among the analytical and numerical modelling results. For partly restrained conditions, the results match satisfactorily.

3.3.3. Interpretation of the results using the concept of degree of freedom

Hinged conditions represent a lower bound of the flexural effects that are likely to characterise plane geostructures. The reason for this is because the rotational stiffness is given only by the presence of the soil. It follows that the soil stiffness plays a paramount role in the definition of flexural behaviour. The stiffer the soil, the lower the deflection and the rotation, the higher the internal actions and the smaller the DOF_c. The softer the soil, the higher the deflection and the rotation, and the lower the internal actions: $DOF_c \rightarrow 1$ when $k_s \rightarrow 0$.

Fully blocked conditions represent an upper bound of the flexural effects that are likely to characterise plane geostructures. In such conditions, rotational and transversal stiffness are blocked by the definition of the boundary conditions (i.e., $DOF_c = 0$). As the deformation is completely blocked for whatever soil stiffness, bending moment reaches its maximum constant value along the beam length as shown in Eq. (8) for $DOF_c = 0$.

Partly restrained conditions represent an intermediate case among hinged and fixed conditions. Consequently, the associated DOF_c lays between the values that characterise beams under fixed and hinged conditions. The definition of DOF_c depends on both the soil and the boundary stiffness. A softer soil allows for higher deflection and rotation, and a flatter distribution of internal actions with respect to a stiffer soil. Regarding the rotational boundary stiffness, the higher k_r, the smaller the deflection and the rotation, and the flatter the distribution of the internal action reaching a constant value while approaching to fixed conditions ($DOF_c \rightarrow 0$).

3.4. Considerations about axial and flexural effects caused by thermal actions

This section aims at providing insights about the modelling of a beam on a Winkler-type soil mass subjected to transversal (i.e., flexural) and axial loads. Transversal loads can be associated, for example, with transversally distributed or concentrated mechanical forces as well as with linear distributions of temperature variations. Axial loads can be associated with axial mechanical forces or constant distributions of temperature variations. Linear distributions of temperature variation induce a transversal action along beams. Constant distributions of temperature variations induce a variation of the deflected shape. The effect of a positive (e.g., tensile) axial load, coming from thermal or mechanical actions reduces the deflection. Conversely, a negative (e.g., compressive) axial load increases the transversal displacement. The limitation of the proposed analytical model is that it is not able to thoroughly quantify axial displacements because of the unidirectional definition (transversal only) of the springs with respect to the beam neutral axis.

4. Application and validation of the analytical model – complex plane geometries

4.1. General

In this section, the proposed extension of Winkler's solution is used

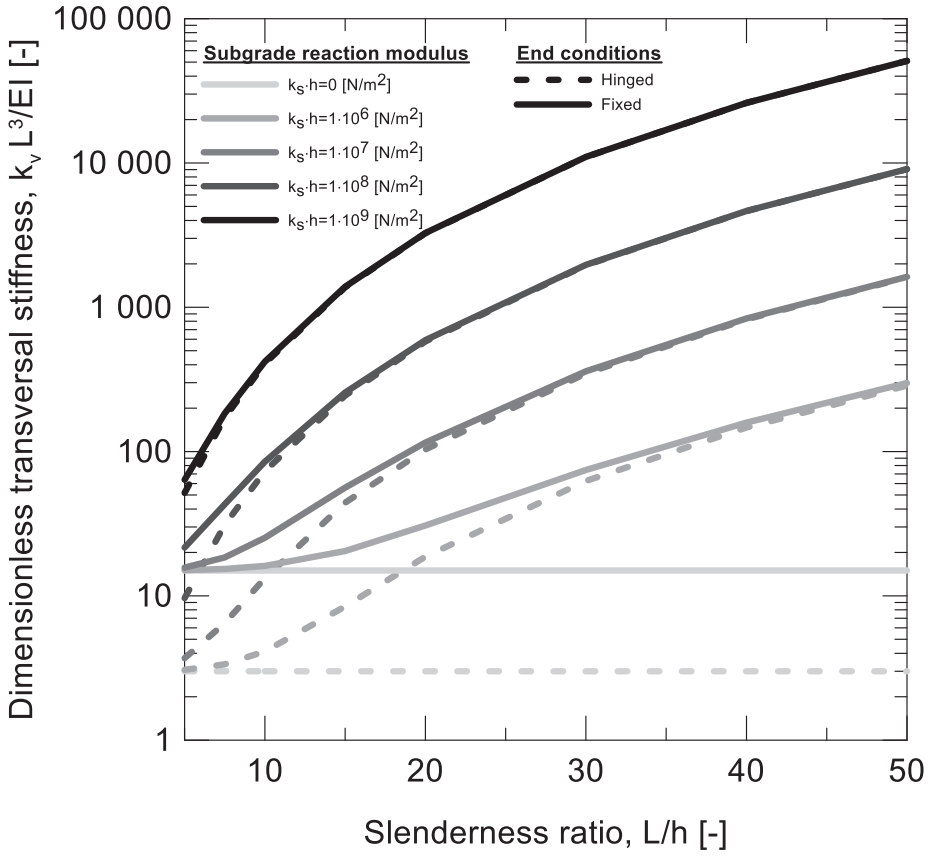

Fig. 10. Relationship between the dimensionless transversal boundary stiffness and the beam geometry.

to investigate the effects of thermal and mechanical actions (e.g., linear distribution of temperature variation and transversal distribution of mechanical load) on the behaviour of a geostructure characterised by a complex plane geometry. While applying the proposed decomposition procedure to the analysis of the considered structure, the main objective of the following developments is to highlight the redistribution of loading conditions within complex plane geometries.

4.2. The problem

A cut-and-cover tunnel with an aspect ratio $L/H = 1$, with $H = L = 10.0$ m, which is embedded in a uniform soil mass, represents the considered complex plane geometry (Fig. 5). Each beam composing the considered geostructure presents a cross-section of $h = B = 1.0$ m. The spring foundation representing the soil mass is characterised by a subgrade reaction modulus of $k_s = 1.8 \times 10^7$ N/m^3. For simplicity, the same value of k_s is considered for the beams lying horizontally and vertically. A detailed treatment of the validity of this assumption is reported elsewhere (Terzaghi, 1955; Balay, 1984; Fages and Bouyat, 1971; Monnet, 1994). The boundary conditions of each beam involve rotational springs of $k_r = 5.0EI/H = 10.4 \times 10^8$ Nm/rad, and transversal springs for horizontal and vertical elements of $k_{v,H} = 30.0EI/L^3 = 6.25 \times 10^7$ N/m and $k_{v,V} = 2.0EA/L = 5.0 \times 10^9$ N/m, respectively. Details on the boundary conditions calibration are reported in Section 4.4.

To address the capabilities of the present analytical model in solving the considered problem, comparisons with the results of numerical models have been made (the details of the numerical models are highlighted in Appendix C). In this context, two problems have been numerically simulated: (i) a cut and cover structure whose response is modelled through beam elements, and a soil whose response is reproduced through spring elements; (ii) a structure whose response is modelled using beam elements and a soil that is modelled as a continuum elastic medium with the elastic parameters calibrated following the formulation proposed by Selvadurai (1979) and Vesic (1961a).

The material constituting the geostructure is reinforced concrete with Young's modulus $E = 25.0$ GPa, Poisson's ratio $\nu = 0.2$ and linear thermal expansion coefficient of $\alpha_{th} = 10^{-5}$ 1/K. The numerical models employing the continuum medium idealisation present the following parameters: $E_s = 2.5 \times 10^7$ N/m^2 and $E_s = 3.5 \times 10^7$ N/m^2 for the one calibrated following (Selvadurai, 1979; Vesic, 1961a), respectively. Poisson's ratio is set to $\nu_s = 0.3$. The applied loading conditions are a linear distribution of temperature variation of $\Delta T_c = 1.0$ °C and a distributed load, downwards directed, acting on the bottom beam of magnitude $q = 1.0$ kN/m. The rationale of considering a linear distribution of temperature variation of $\Delta T_c = 1.0$ °C applies to the consideration of a distributed mechanical load of $q = 1.0$ kN/m.

4.3. Analysis approach

This section expands on the steps allowing to model complex plane geometries such as a cut-and-cover tunnel using the proposed analytical model and the decomposition analysis approach. The considered cut-and-cover structure can be decomposed in four single beams. Boundary conditions and loading conditions for each beam have to be detailed to ensure continuity and a correct redistribution of actions throughout the structure.

The solution method is based on five steps (Table 4). Step 1: the equilibrium of the bottom beam (1) is solved considering q and ΔT_c. Step (2): the equilibrium of beam (2) is solved by imposing the rotation and the shear force coming from beam (1) at one boundary (the shear force for beam (2) represents the axial force for beam (1)). Step 3: the same procedure considered in Step 2 is applied to resolve the equilibrium of beam (3). Step 4: the equilibrium of beam (1) is re-assessed by

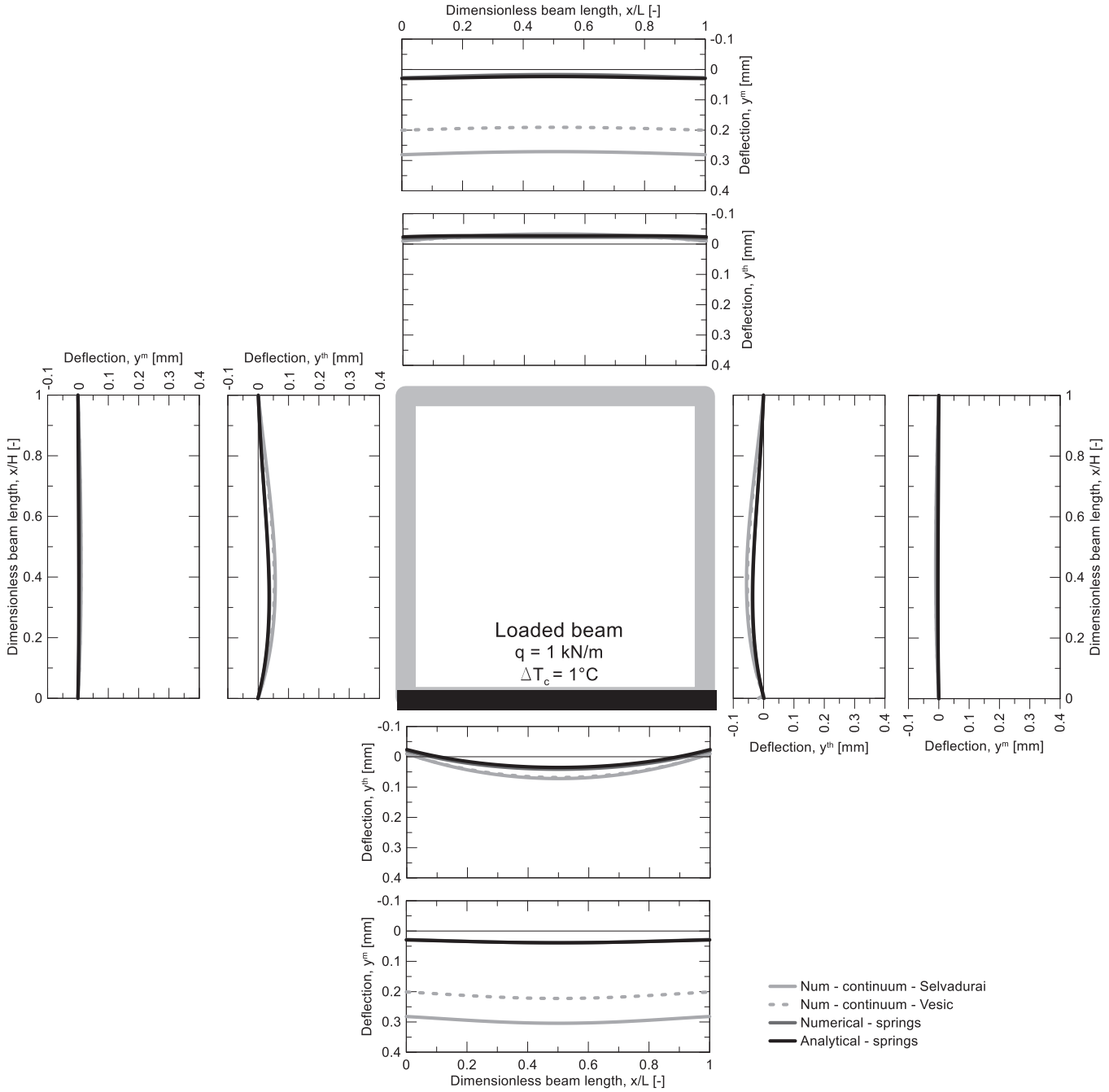

Fig. 11. Response of a cut-and-cover structure with $L/H = 1$ subjected to thermal and mechanical loading to the bottom beam only: deflection.

adding the axial action coming from the shear force distribution in beams (2) and (3). Step 5: the upper beam (4) is solved by imposing rotations coming from beams (2) and (3) and transversal displacements coming from beam (1) (assuming that beams (2) and (3) settle/heave as rigid bodies). Such boundary conditions lead to a discontinuity in bending moment between beams (2), (3) and (4), , but this discrepancy tends to zero, ensuring a suitable calibration of the boundary conditions (rotational and transversal stiffness). For this reason, in the following, a procedure for estimating and calibrating the boundary conditions is proposed.

It is worth noting that the foregoing analysis approach could be applied to any arbitrary loading scenario and plane geometry. For example, a slightly more complex problem than the one considered here could consist in a cut-and-cover structure with more than one beam subjected to thermal actions. Such a problem may be adequately addressed following a similar procedure than the one described above.

4.4. Calibration of boundary conditions

In this section, a procedure for calibrating the rotational and transversal stiffness to be employed in boundary conditions is presented. Such a procedure aims to be as general as possible, so that it may be used to tackle frequent problems in engineering when different variably connected elements are present (e.g., perpendicular and variably inclined connections, wall-anchors, etc). In the following, two components of stiffness are considered: the structural (subscript “SS”) and the soil-structure interaction (subscript “SSI”).

4.4.1. Rotational stiffness

The structural stiffness, $k_{r,SS}$, is related to the frame rigidity and can

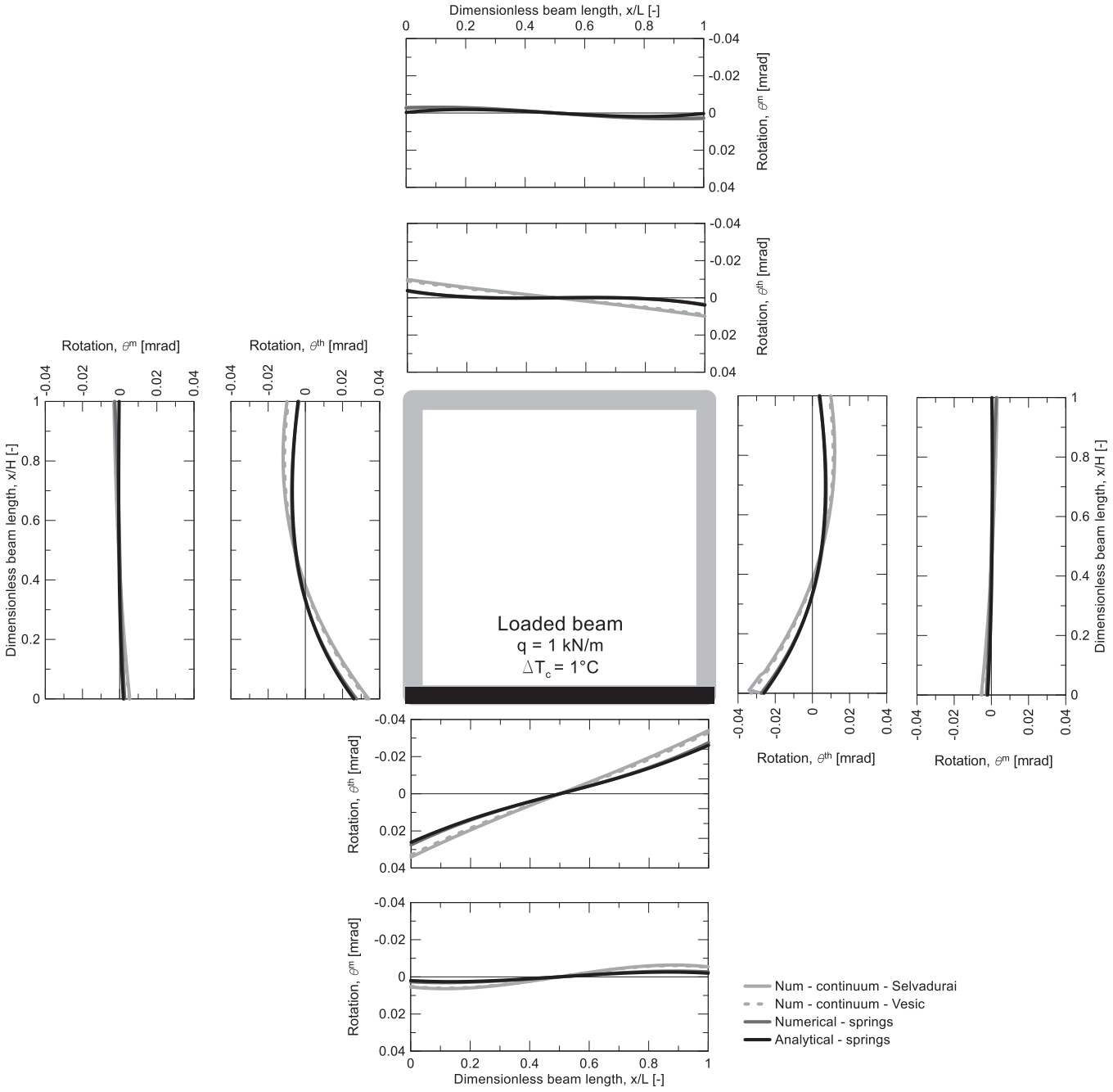

Fig. 12. Response of a cut-and-cover structure with $L/H = 1$ subjected to thermal and mechanical loading to the bottom beam only: rotation.

be determined by employing the so-called displacement method, as described in Connor and Faraji (2016). This method is employed here with reference to the structure shown in Fig. 7(a)–(c). The value of $k_{r,SS}$ is bounded by an upper bound (fixed condition) and a lower bound (hinged condition). The upper bound relates to a case where the rotation is blocked by the presence of a fixed end. The bending moment M^* applied at the frame angle induces a rotation of $M^*(4EI/L)^{-1}$ radians. The stiffness of the equivalent rotational spring is therefore $4.0EI/L$ Nm/rad (Fig. 7(a)). The lower bound is characterised by the beam hinged at its ends (Fig. 7(b)). The equivalent rotational stiffness is thus $3.0EI/L$ Nm/rad. It follows that if the rotation is partly restrained, the spring structural stiffness reads (Fig. 7(c))

$$k_{r,SS} = \frac{m^* EI}{L} \quad \text{with} \quad m^* = 3.0 \div 4.0 \tag{26}$$

The whole structure is also constrained by the presence of soil all around, which is partly restraining the rotations. The rotational stiffness $k_{r,SSI}$ is the one exerted by the soil-structure interaction in the portions not accounting for the beam of interest. This contribution can be estimated by applying a unit moment, M^*, to a beam that is fixed at one end and supported by the spring foundation along its length (Fig. 7(d) and (e)). A first estimation of $k_{r,SSI}$, $k_{r,1}$, can be obtained by dividing the unit moment M^* by the rotation θ_1 and subtracting the structural flexural stiffness, equal to EI/L for this case (Fig. 7(d)). The final evaluation of $k_{r,SSI}$ is done by applying the same method to the structure with a replacement of the fixed end with a rotational spring of stiffness $k_{r,1} + k_{r,SS}$ (Fig. 7(e)).

The equivalent rotational spring, k_r, can be estimated by summing the two components previously highlighted:

$$k_r = k_{r,SS} + k_{r,SSI} \tag{27}$$

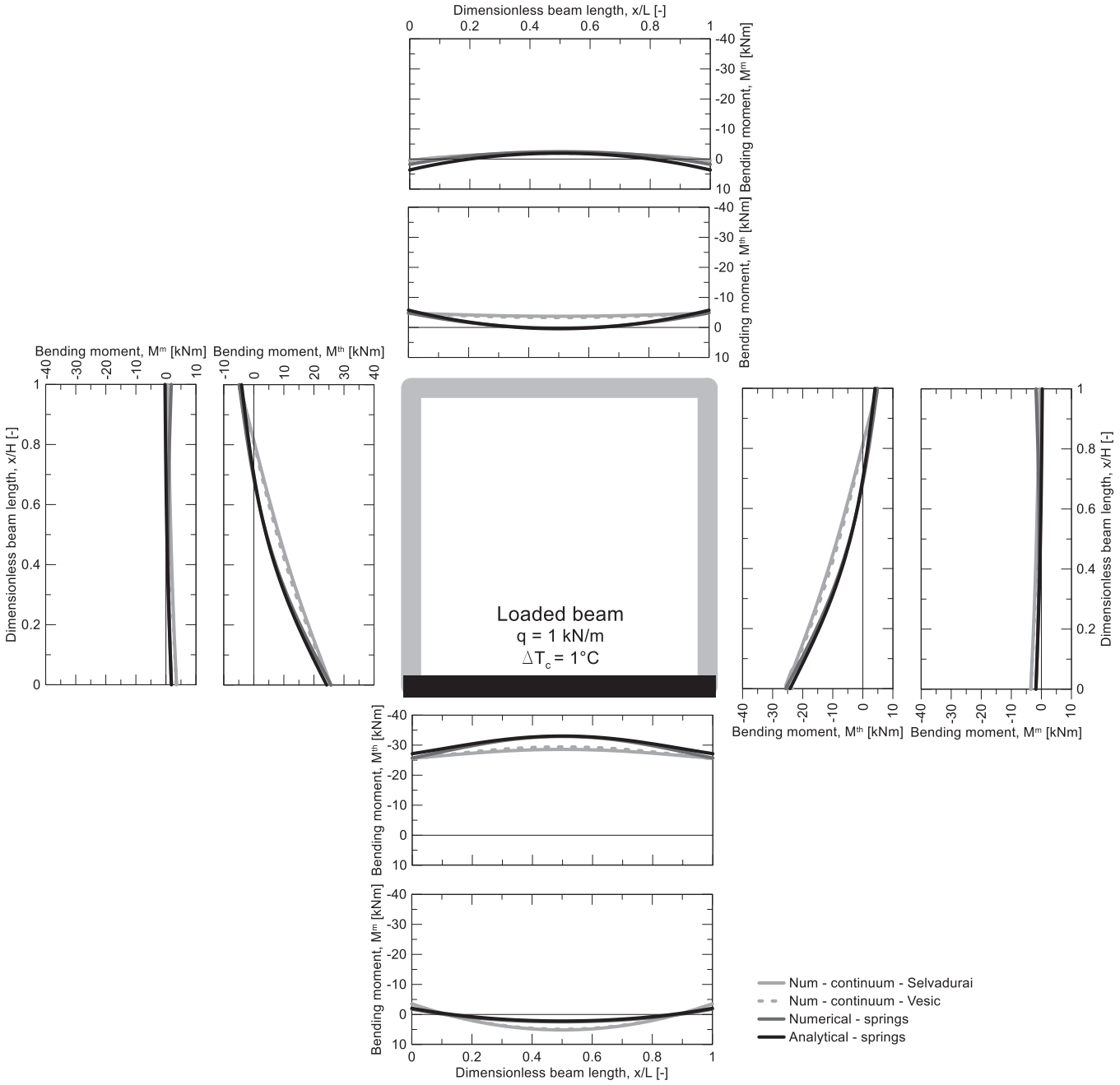

Fig. 13. Response of a cut-and-cover structure with $L/H = 1$ subjected to thermal and mechanical loading to the bottom beam only: bending moment.

Fig. 8 shows the relationship between the dimensionless rotational stiffness and the beam geometry. Each line in the plot contains the sum of the evaluations described in Fig. 7, providing upper and lower bounds for different soils. In all cases, the soil subgrade reaction modulus, k_s, is multiplied by the beam height, h, to give results that are independent to the beam height. The results depicted for $k_s h = 0$ N/m^2 include the stiffness given by the structure only. The difference between these results and those obtained for $k_s h \neq 0$ N/m^2 denotes the contribution of the soil-structure interaction.

4.4.2. Transversal stiffness

The evaluation of the transversal stiffness has to account for four components (Fig. 9(a)): the bottom connection, $k_{v,c1}$, the axial stiffness of the structural element, $k_{v,a}$, the top connection, $k_{v,c2}$, and the soil-structure interaction, $k_{v,SSI}$. Such components can be represented by four springs in series. This approach yields to the following formulation of the equivalent transversal stiffness, k_v:

$$k_v = \frac{1}{\frac{1}{k_{v,a}} + \frac{1}{k_{v,C1}} + \frac{1}{k_{v,C2}} + \frac{1}{k_{v,SSI}}} \tag{28}$$

As Winkler's solution does not consider any friction between the soil and the structure, this aspect is neglected. $k_{v,a}$ relates to the axial stiffness of a beam as follows:

$$k_{v,a} = \frac{EA}{L} \tag{29}$$

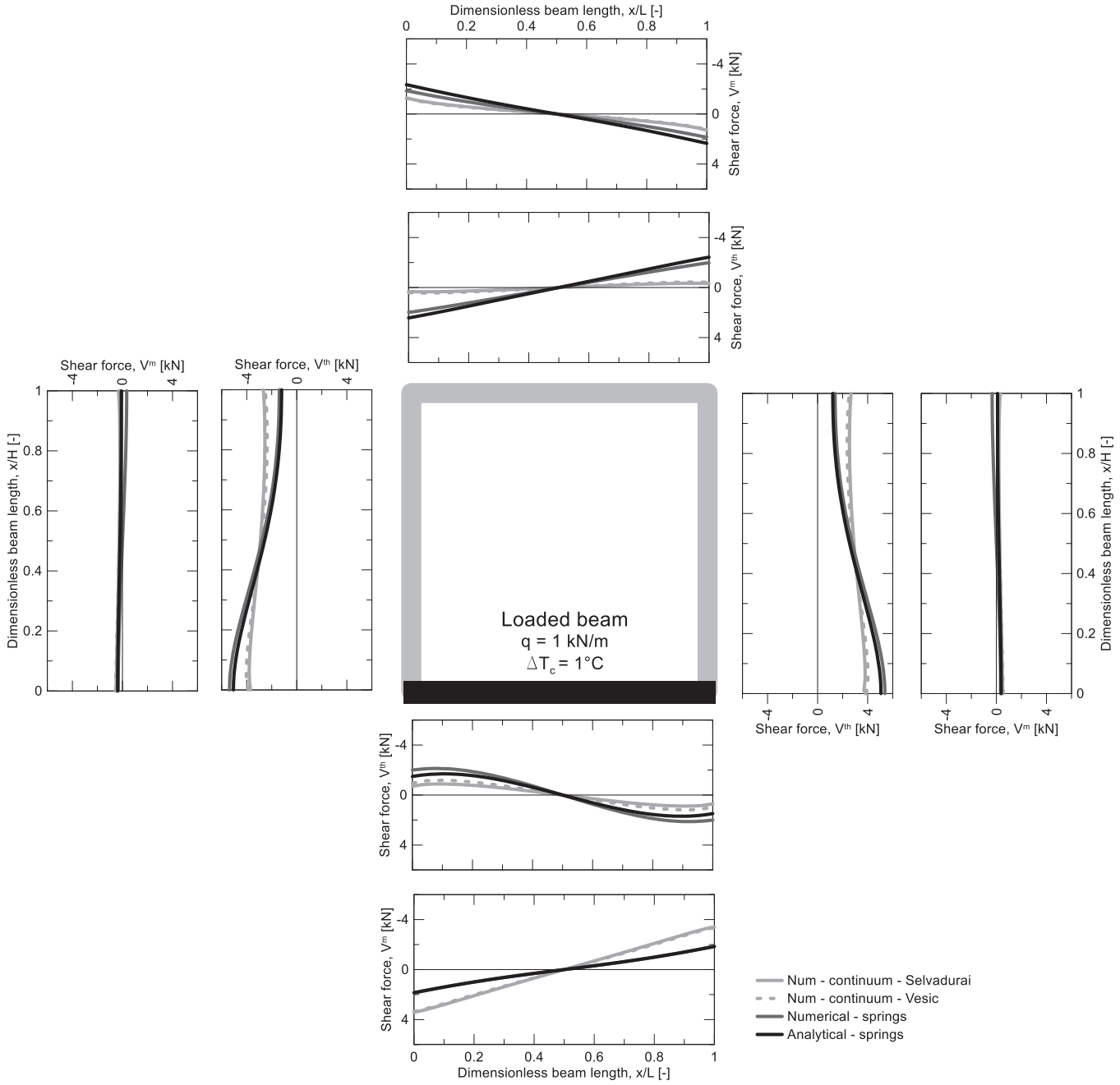

Fig. 14. Response of a cut-and-cover structure with $L/H = 1$ subjected to thermal and mechanical loading to the bottom beam only: shear force.

In many cases, $k_{v,a}$ is considerably higher with respect to the other components, hence it can often be neglected in Eq. (28): depending on the geometry details, such element may behave as a rigid body that is not deforming axially, but it only transfers the loads to the surrounding structures. $k_{v,c1}$ and $k_{v,c2}$ can be determined by considering the following upper and lower bound cases (Fig. 9(b)–(d)). The upper bound is represented by the stiffer case (fixed ends, Fig. 9(b)), while the lower bound involves free rotation at the ends (hinged ends, Fig. 9(c)). Following the same methodology shown for the rotational spring, it follows that the connection stiffness, $k_{v,ci}$, can be evaluated as (Fig. 9(d)):

$$k_{v,ci} = v^* \frac{EI}{L^3} \quad \text{with} \quad i = 1,\ 2 \quad \text{and} \quad v^* = 1.5 \div 7.5 \tag{30}$$

For the determination of the soil-structure interaction vertical stiffness, different methodologies should be employed for the analysis of (i) the horizontal beams and of (ii) the vertical walls. For horizontal beams, $k_{v,SSI}$ is estimated by considering the static scheme shown in Fig. 9(e) and (f). The first step is to consider a beam fixed at one end and subjected to a unit transversal load, P^*. $k_{v,1}$ is evaluated by dividing P^* by the correspondent vertical displacement, y_1, and subtracting the structural transversal stiffness, $3.0EI/L^3$. The second and final step is to consider the same beam solved by replacing the fixed boundary with $k_{v,1}$and k_r, (Fig. 9(f)). The vertical stiffness for the second step, $k_{v,2}$ can be similarly evaluated. It follows that

$$k_{v,SSI} = k_{v,2} \tag{31}$$

For vertical beams, the determination of their transversal boundary stiffness is based on their mechanical response. In the considered problem, the two vertical beams behave symmetrically. Their transversal boundary stiffness can therefore be estimated as the axial stiffness of a half of a horizontal beam.

$$k_{v,vertical} = \frac{EA}{L/2} \tag{32}$$

Fig. 10 shows the estimation of k_v through the relationship between the transversal stiffness and the geometry details. This chart includes the steps described in Fig. 9(b)–(e). Only the case $k_{v,c1} = k_{v,c2}$ is included in the charts. The soil subgrade reaction modulus, k_s, is multiplied by the beam height, h, to give results that are independent to the beam height.

The results depicted for $k_s h = 0$ N/m^2 include the stiffness given by the structure only. The difference between these results and those obtained for $k_s h \neq 0$ N/m^2 denotes the contribution of the soil-structure interaction.

4.5. Comparison between analytical and numerical modelling results

In the following, the response of the modelled cut-and-cover structure is addressed with reference to the considered action effects (depicted for each portion of the structure), by distinguishing the influence of thermal and mechanical actions.

Deflections are shown in Fig. 11. A close correspondence between the analytical and numerical modelling results is observed when addressing the influence of the thermal load. The predicted structural response is in fact very similar in all cases, highlighting a slight underestimation of the deflections only when considering the spring foundation models (numerical and analytical). Due to the end stiffness definition, the deflections of the lower beam are minimal (lower than 0.1 mm). Due to the downward bending of the lower beam, the two walls displace towards the inner part of the structure, while the upper beam moves upward. The whole structure slightly moves upward due to the soil reaction against the lower beam. A more significant difference between the analytical and numerical modelling results is observed when addressing the influence of the mechanical load. The spring foundation models considerably underestimate the horizontal beam displacements. The shape of the deflection is similar, thus confirming that Winkler's solution can be used to estimate the differential settlements of footings, but is unsuitable to thoroughly capture actual settlements, especially when dealing with particularly rigid structures.

Rotations are shown in Fig. 12. A close correspondence between the analytical and numerical modelling results is observed when addressing the influence of both the thermal and mechanical load. The analytical and numerical modelling results with spring foundation slightly underestimate rotations. The thermal load affects rotations in the whole structure, thus inducing much higher rotations at the edges of the cut-and-cover with respect to the distributed mechanical load. The distributed mechanical load induces a flatter displacement profile, hence involving rotations that are very small compared to those caused by thermal loading.

Bending moments are shown in Fig. 13. A close correspondence between the analytical and numerical modelling results is observed when addressing the influence of both the thermal and mechanical loads. The thermal load induced a rotation that is notably restrained at the boundaries, while a bending moment distribution that is flatter but high in magnitude, with values higher compared to the distributed load. Models with spring foundation slightly overestimate internal actions in the bottom beam. The mechanical load induces a bending moment that is nearly-zero, hence the thermal load is determining significant effects in the structure.

Shear forces are detailed in Fig. 14. A satisfactory correspondence among the analytical and numerical modelling results is recorded for thermal and mechanical loads. The thermal load causes shear actions in the entire structure, consequently to the bending moment distribution. The distributed load induces shear forces only in the horizontal beams due to the nature of the applied load (transversal to horizontal beams). The sign of shear action induced by ΔT_c is opposite to that of q. It follows that they delete each other. However, if the thermal load takes the opposite sign, the total shear force would sum the two.

5. Concluding remarks

This study aims at taking a step forward towards a detailed assessment of the thermo-mechanical behaviour of plane geostructures subjected to thermal and mechanical actions by proposing an analytical model for capturing the effects of the considered perturbations. The proposed model extends Winkler's solution to non-isothermal conditions for quantifying the effects of actions that include, without being limited to, temperature variations, axial loads, transversal loads and bending moments applied to plane geostructures resting on an elastic soil mass. The model formulation resorts to a theoretical analysis of the influence of thermal and mechanical actions applied to geostructures, as well as to a new definition of degree of freedom for capturing the influence of axial and flexural effects caused by thermal actions.

By resorting to novel charts and mathematical procedures that can be employed to calibrate appropriate boundary conditions for the analysis of simple and complex plane geostructures, the work highlights aspects of paramount importance for the modelling of plane earth-contact structures. A comparison between analytical and numerical modelling results highlights that the proposed extension of Winkler's solution can capture with accuracy problems of varying complexity as long as similar hypotheses are employed in the analyses. This work provides a tool based on sound principles of mechanics for both scientific and engineering investigations, enabling a novel approach to tackle the analysis of plane geostructures subjected to thermal and mechanical actions.

CRediT authorship contribution statement

Jacopo Zannin: Conceptualization, Validation, Writing - original draft, Visualization. **Alessandro F. Rotta Loria:** Conceptualization, Validation, Writing - original draft, Visualization. **Qazim Llabjani:** Conceptualization, Methodology, Software, Formal analysis, Investigation, Visualization. **Lyesse Laloui:** Validation, Writing - review & editing, Supervision, Project administration.

Declaration of Competing Interest

The authors declare that they have no known competing financial interests or personal relationships that could have appeared to influence the work reported in this paper.

Appendix A

This appendix expands on critical features of the method of initial conditions, as remarked by Hétenyi (1946) and Selvadurai (1979). The method of initial conditions is powerful for solving the case of generally loaded beams. This method consists in replacing the integration constants with the four conditions at the origin of the beam (x= 0): y_0, ϑ_0, M_0 and V_0. The general solution of the elastic line, in the case with axial load, is presented here. The fourth-order differential equation to be solved is:

$$EI\frac{d^4y(x)}{dx^4} - N\frac{dy(x)}{dx} + k_s y(x) = 0 \tag{A.1}$$

The general solution of the deflection is:

$$y(x) = (C_1 e^{\alpha x} + C_2 e^{-\alpha x})\cos\beta x + (C_3 e^{\alpha x} + C_4 e^{-\alpha x})\sin\beta x \tag{A.2}$$

where

$$\alpha = \sqrt{\sqrt{\frac{k}{EI}} + \frac{N}{4EI}} = \sqrt{\lambda^2 + \frac{N}{4EI}} \tag{A.3}$$

$$\beta = \sqrt{\sqrt{\frac{k}{EI}} - \frac{N}{4EI}} = \sqrt{\lambda^2 - \frac{N}{4EI}} \tag{A.4}$$

The values of $y(x)$ and its derivatives at $x = 0$ are:

$$y(0) = y_0 = C_1 + C_2 \tag{A.5}$$

$$\frac{dy(0)}{dx} = \theta_0 = \alpha(C_1 - C_2) + \beta(C_3 + C_4) \tag{A.6}$$

$$-EI\frac{d^2y(0)}{dx^2} = M_0 = EI\left[\beta^2(C_1 + C_2) - \alpha^2(C_1 + C_2) - 2\alpha\beta(C_3 - C_4)\right] \tag{A.7}$$

$$-EI\frac{d^3y(0)}{dx^3} = V_0 = -EI\left[-\beta^3(C_3 + C_4) + \alpha^3(C_1 - C_2) - 3\alpha\beta^2(C_1 - C_2) + 3\alpha^2\beta(C_3 + C_4)\right] \tag{A.8}$$

The unknowns C_1 to C_4 become:

$$C_1 = \frac{1}{2}y_0 - \frac{\beta^2 - 3\alpha^2}{4\alpha(\beta^2 + \alpha^2)}\theta_0 + \frac{1}{4EI\alpha(\beta^2 + \alpha^2)}V_0 \tag{A.9}$$

$$C_2 = \frac{1}{2}y_0 + \frac{\beta^2 - 3\alpha^2}{4\alpha(\beta^2 + \alpha^2)}\theta_0 - \frac{1}{4EI\alpha(\beta^2 + \alpha^2)}V_0 \tag{A.10}$$

$$C_3 = \frac{\beta^2 - \alpha^2}{4\alpha\beta}y_0 + \frac{3\beta^2 - \alpha^2}{4\beta(\beta^2 + \alpha^2)}\theta_0 - \frac{1}{4EI\alpha\beta}M_0 - \frac{1}{4EI\beta(\beta^2 + \alpha^2)}V_0 \tag{A.11}$$

$$C_4 = \frac{\alpha^2 - \beta^2}{4\alpha\beta}y_0 + \frac{3\beta^2 - \alpha^2}{4\beta(\beta^2 + \alpha^2)}\theta_0 + \frac{1}{4EI\alpha\beta}M_0 - \frac{1}{4EI\beta(\beta^2 + \alpha^2)}V_0 \tag{A.12}$$

The general equation for the deflection, following the method of initial conditions (Hétenyi, 1946) becomes:

$$y(x) = y_0F_1(x) + \theta_0F_2(x) - \frac{1}{EI}M_0F_3(x) - \frac{1}{EI}V_0F_4(x) \tag{A.13}$$

with:

$$F_1(x) = cosh\alpha x\cos\beta x + \sinh\alpha x\sin\beta x\left(\frac{\beta^2 - \alpha^2}{2\alpha\beta}\right) \tag{A.14}$$

$$F_2(x) = \frac{1}{2(\alpha^2 + \beta^2)}\left[cosh\alpha x\sin\beta x\left(\frac{3\beta^2 - \alpha^2}{\beta}\right) - \sinh\alpha x\cos\beta x\left(\frac{\beta^2 - 3\alpha^2}{\alpha}\right)\right] \tag{A.15}$$

$$F_3(x) = \frac{1}{2\alpha\beta}[\sinh\alpha x\sin\beta x] \tag{A.16}$$

$$F_4(x) = \frac{1}{2(\alpha^2 + \beta^2)}\left[\frac{cosh\alpha x\sin\beta x}{\beta} - \frac{\sinh\alpha x\cos\beta x}{\alpha}\right] \tag{A.17}$$

Appendix B

This appendix expands on key features of methods for determining the modulus of subgrade reaction. The evaluation of k_s is presented referring to a practical application for a horizontal geostructure made of reinforced concrete with Young's modulus of $E = 25.0$ GPa, a cross-section height of $h = 0.5$ m, breadth of $B = 1.0$ m and length of $L = 10.0$ m. Results are presented in Fig. 15. The geostructure is assumed to rest on a uniform soil with Poisson's ratio of $\nu_s = 0.3$ and a varying Young's modulus between $E_s = 10^6 \div 10^8$ N/m^2. A sensitivity analysis on ν_s indicates that this parameter induces minimal differences in the estimates of k_s.

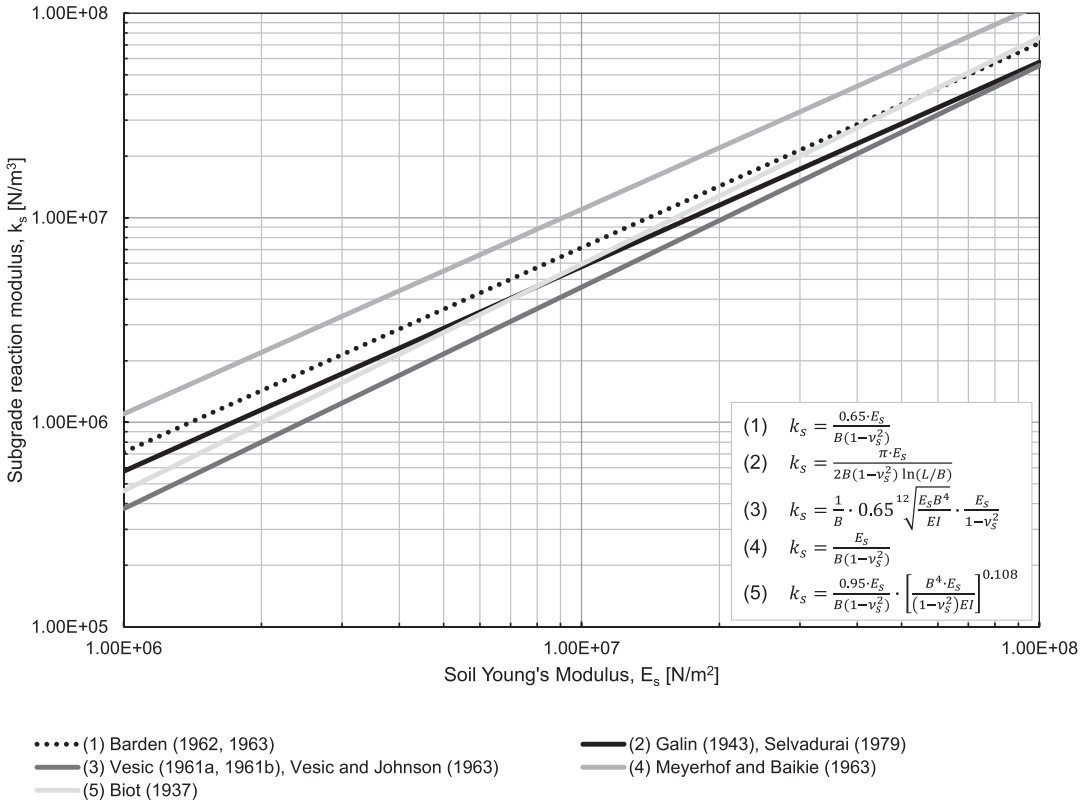

Fig. 15. Evaluation of the subgrade reaction modulus based on empirical formulations.

Appendix C

This appendix expands on key features of the numerical analyses and models employed in this paper to validate the proposed analytical models. The numerical models employing spring foundations are a numerical resolution of the analytical model presented here.

The numerical models employing a linear elastic soil mass are described here. Two-dimensional (2D) plane strain thermo-mechanical finite element models are built using Comsol Multiphysics for the considered purpose. In these models, the soil is modelled as a linear elastic medium. This approach involves considering the soil as an infinite heat reservoir that remains at a fixed constant temperature. While approximate, this assumption agrees with the hypotheses and features of the Winkler's solution extended in this work and finds due justification in the works of (Rotta Loria and Laloui, 2016, 2017; Rotta Loria et al., 2018). In this model, the geostructure is modelled with beam elements that follow Euler-Bernoulli theory while the soil mass follows continuum mechanics.

The behavior of the beam elements is described through structural mechanics' theory, by employing the Euler-Bernoulli theory of beams. The beam is considered to be isotropic and homogeneous and the mechanical behavior is described through Navier formulation for bending of beams:

$$\sigma_n(y_n) = \frac{N}{A} + \frac{M}{I} y_n \tag{C.1}$$

where $\sigma_n(y_n)$ represents the bending stress and y_n the distance to the neutral axis.

Following linear elasticity, the axial, bending moment and shear force can be written as:

$$N(x) = EA\frac{du}{dx} \tag{C.2}$$

$$M(x) = EI\frac{\partial^2 y}{\partial x^2} \tag{C.3}$$

$$V(x) = EI\frac{\partial^3 y}{\partial x^3} \tag{C.4}$$

where u represents the axial displacement.

A linear distribution of temperature variation can be applied by imposing a thermal curvature to the beam:

$$\chi^{th} = \frac{2\alpha_{th}\Delta T_c}{h} \tag{C.5}$$

A mechanical load can be applied as a boundary load transversal to the beam's neutral axis.

The soil is modelled as a linear-elastic continuum, allowing for considering the portion of soil surrounding the beam. Winkler's solution (e.g., the analytical model proposed in this study) models the soil as unidirectional independent springs that present a linear elastic relation among load and displacement. Consequently, Winkler solution is not capable of capturing the behaviour of the materials surrounding the studied structural element. No heat transfer in the soil is considered in the numerical models. The mechanical behaviour of the continuum media is described by the following

equations. The equilibrium equation reads:

$$div\sigma_{ij} + \rho g_i = 0 \tag{C.6}$$

where div denotes the divergence operator, σ_{ij} is the total stress tensor, ρ the bulk density of the material and g_i is the gravity acceleration vector.

The constitutive law, in the incremental form reads:

$$d\sigma_{ij} = C_{ijkl} d\varepsilon_{kl} \tag{C.7}$$

in which C_{ijkl} is the constitutive tensor and ε_{kl} is the total strain tensor.

At the beam-soil interface, continuity of displacement is imposed:

$$u_{S,i} = u_{B,i} \quad on \quad \Omega_S \cap \Omega_B \tag{C.8}$$

where $u_{S,i}$ and $u_{B,i}$ represent the soil and beam displacement vector, respectively. Ω_S and Ω_B are the edges of soil and beam domains. The numerical models are detailed in Fig. 16.

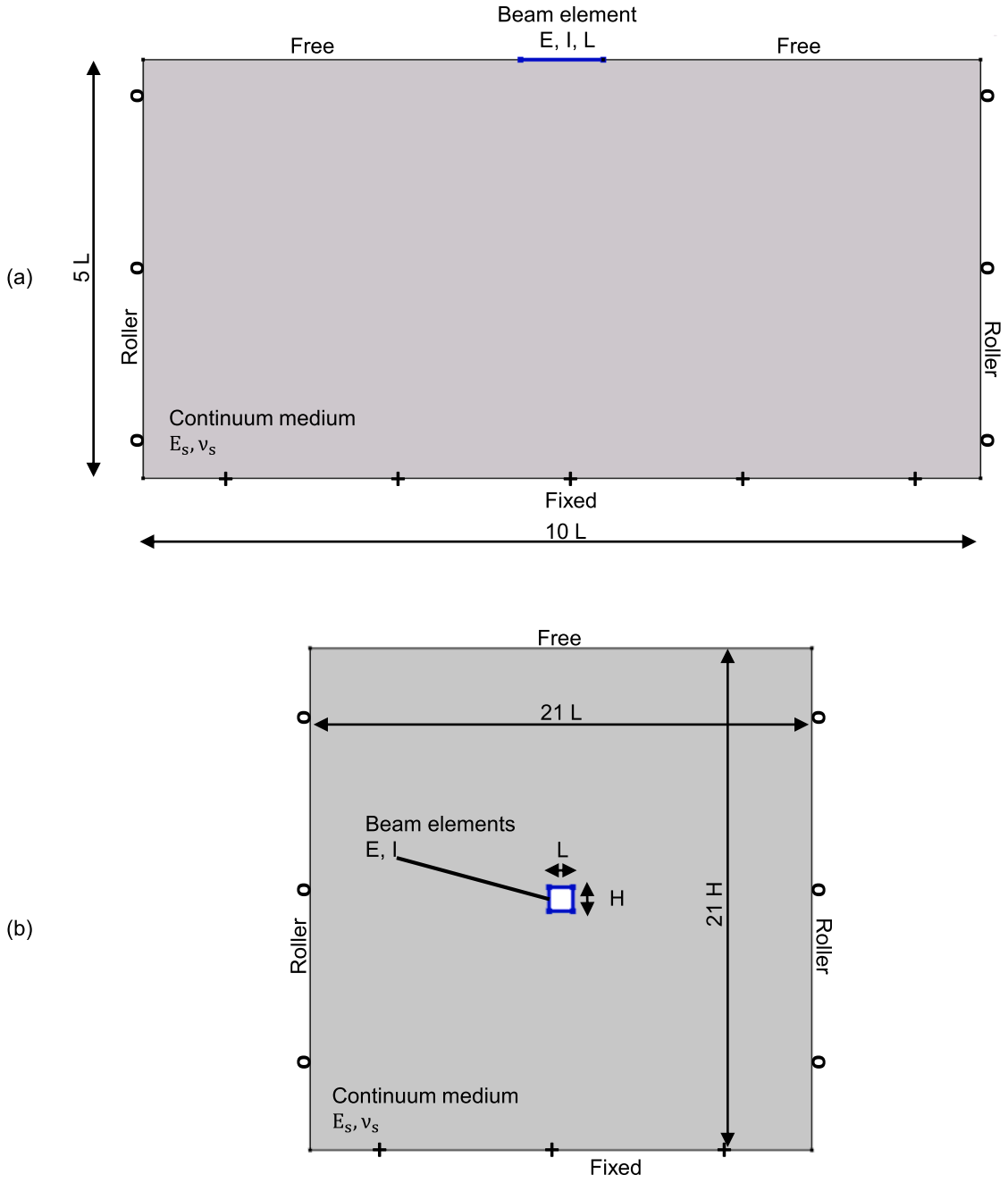

Fig. 16. Features of the numerical models: (a) a beam on an elastic continuum material and (b) a cut-and-cover tunnel in an elastic continuum material.

References

Balay J. Recommandations pour le choix des paramètres de calcul des écrans de soutènement par la methode aux modules de reaction. Note Inf. Tech. Lab. Cent. Ponts Chausees LCPC; Jul. 1984.

Barden, L., 1962. Distribution of contact pressure under foundations. Géotechnique 12 (3), 181–198. https://doi.org/10.1680/geot.1962.12.3.181.

Barden, L., 1963. The Winkler model and its application to soil. Str. Eng. 9 (41), 279–280.

Biot, M., 1937. Bending of an infinite beam on an elastic substrate. ASME J Appl Mech 4, A1–A7.

Bourne-Webb, P.J., Bodas Freitas, T.M., da Costa Gonçalves, R.A., 2016. Thermal and mechanical aspects of the response of embedded retaining walls used as shallow geothermal heat exchangers. Energy Build 125, 130–141. https://doi.org/10.1016/j.enbuild.2016.04.075.

COMSOL Inc. (s.d.)., COMSOL Multiphysics Reference Manual, version 5.3. www.comsol.com.

Coulomb. Essai sur une application des regles de maximis et minimis a quelques problemes de statique, relatifs a l'architecture, vol. 1. Paris: Memoires de Mathematique et de Physique présentés a l'Academic Royale des Sciences, 1776.

Connor, J., Faraji, S., 2016. Fundamentals of structural engineering. Springer.

Coyle, H.M., Reese, L.C., 1966. Load transfer for axially loaded piles in clay. J Soil Mech Found Div 92 (2), 1–26.

Delattre, L., 2001. Un siecle de methodes de calcul d'ecrans de soutenement. I. L'approche par le calcul - les methodes classiques et la methode au coefficient de reaction. Bull Lab Ponts Chaussées 234.

Fages R, Bouyat C. Calcul des rideaux de parois moulées ou de palplanches. Modèle mathematique integrant le comportement irreversible du sol en état élasto-plastique. Travaux, no. 439; Oct. 1971.

Frank R, Zhao S. Estimation par les paramètres pressiometriques de l'enfoncement sour charge axiale des pieux forés dans des sols fins. Bull Liaison Lab Ponts Chauss, no. 119; May 1982.

Galin, L., 1943. On the Winkler-Zimmermann hypothesis for beams (in Russian). Prikl Mat Mekh 7 (4), 293–300.

Hétenyi, M., 1946. Beams on elastic foundations Theory with applications in the fields of civil and mechanical engineering. The University of Michigan Press, Ann Arbor.

Hétenyi, M., 1950. A general solution for the bending of beams on an elastic foundation of arbitrary continuity. J Appl Phys 1 (21), 55–58. https://doi.org/10.1063/1.1699420.

Kerr, A.D., 1965. A study of a new foundation model. Acta Mech. 1 (2), 135–147. https://doi.org/10.1007/BF01174308.

Laloui, L., Rotta Loria, A.F., 2019. Analysis and design of energy geostructures, 1st ed. Elsevier Academic Press.

Laloui, L., Moreni, M., Vulliet, L., 2003. Comportement d'un pieu bi-fonction, fondation et échangeur de chaleur. Can Geotech J 40 (2), 388–402. https://doi.org/10.1139/t02-117.

Monnet, A., 1994. Module de réaction, coefficient de décompression, au sujet des paramètres utilisés dans la méthode de calcul élasto-plastique des soutènements. Rev Fr Géotechnique 66, 67–72. https://doi.org/10.1051/geotech/1994066067.

Ménard L, Bourdon C. Calcul des rideaux de soutènement. Méthode nouvelle prenant en compte les conditions réelles d'encastrement. Sols-Soils no. 12; 1965.

Meyerhof, G.G., Baikie, L.D., 1963. Strength of steel culvert sheets bearing against compacted sand backfill. Highway Research Board, Proceedings of the 42nd Annual Meeting.

Pasternak, P., 1954. On a new method of analysis of an elastic foundation by means of two foundation constants. Gosudarstvennoe Izdatelstro Liberaturi po Stroitelstvui Arkhitekture, Moscow.

Reissner, M.E., 1937. On the theory of beams resting on a yielding foundation. Proc Natl Acad Sci USA 23 (6), 328–333.

Rotta Loria, A.F., Laloui, L., 2016. The interaction factor method for energy pile groups. Comput. Geotech. 80 (Dec.), 121–137. https://doi.org/10.1016/j.compgeo.2016.07.002.

Rotta Loria, A.F., Laloui, L., 2017. Displacement interaction among energy piles bearing on stiff soil strata. Comput. Geotech. 90 (Oct.), 144–154. https://doi.org/10.1016/j.compgeo.2017.06.008.

Rotta Loria AF, Laloui L. Thermo-mechanical schemes for energy piles. In: Energy Geotechnics, Cham, 2019. p. 218–25. https://doi.org/10.1007/978-3-319-99670-7_28.

Rui, Y., Yin, M., 2018. Thermo-hydro-mechanical coupling analysis of a thermo-active diaphragm wall. Can Geotech J 55 (5), 720–735. https://doi.org/10.1139/cgj-2017-0158.

Rotta Loria, A.F., Vadrot, A., Laloui, L., 2018. Analysis of the vertical displacement of energy pile groups. Geomech Energy Environ 16 (Dec.), 1–14. https://doi.org/10.1016/j.gete.2018.04.001.

Schmitt, P., 1995. Méthode empirique d'évaluation du coefficient de réaction du sol vis-à-vis des ouvrages de soutènement souples. Rev Fr Géotechnique 71, 3–10. https://doi.org/10.1051/geotech/1995071003.

Selvadurai, A.P.S., 1979. Elastic analysis of soil-foundation interaction, vol. 17 Elsevier Scientific Publishing Company, Amsterdam.

Sailer, E., Taborda, D.M.G., Zdravkovic, L., Potts, D.M., 2019. Fundamentals of the coupled thermo-hydro-mechanical behaviour of thermo-active retaining walls. Comput Geotechn 109, 189–203. https://doi.org/10.1016/j.compgeo.2019.01.017.

Sterpi, D., Coletto, A., Mauri, L., 2017. Investigation on the behaviour of a thermo-active diaphragm wall by thermo-mechanical analyses. Geomech Energy Environ 9, 1–20. https://doi.org/10.1016/j.gete.2016.10.001.

Terzaghi K. Evaluation of coefficients of subgrade reaction. Geotechnique 1955;4(5).

Truesdell C. The rational mechanics of flexible or elastic bodies 1638–1788. Leonhardi Euleri Opera Omnia, Ser. 2. Turici : Venditioni exponunt Orell Füssli(IS), Zürich: Füssli; 1960.

Vesic, A.B., 1961a. Bending of beams resting on isotropic elastic solid. J Eng Mech Div Proc ASCE 87 (EM2), 35–53.

Vesic A. Beams on elastic subgrade and Winkler's hypothesis. In: Proc. 5th Int. Conf. Soil Mech. Found. Eng., no. 1; 1961b. p. 845–50.

Vesic, A., Johnson, W., 1963. Model studies of beams resting on a silt subgrade. J Soil Mech Found Div Proc ASCE 89 (SM1), 1–31.

Winkler, E., 1867. Die Lehre von der elasticitaet und festigkeit. Prag Dominicus, Berlin.

Wolfram Research. Wolfram Language & System Documentation Center; 2019.